Accepted Manuscript

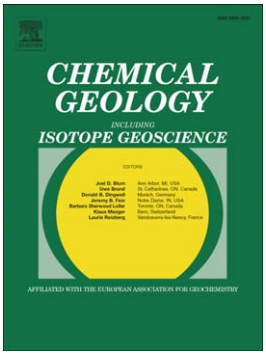

Discerning primary versus diagenetic signals in carbonate carbon and oxygen isotope records: An example from the Permian–Triassic boundary of Iran

Martin Schobben, Clemens Vinzenz Ullmann, Lucyna Leda, Dieter Korn, Ulrich Struck, Wolf Uwe Reimold, Abbas Ghaderi, Thomas J. Algeo, Christoph Korte

PII: S0009-2541(15)30133-9
DOI: doi: 10.1016/j.chemgeo.2015.12.013
Reference: CHEMGE 17794

To appear in: *Chemical Geology*

Received date: 27 July 2015
Revised date: 28 October 2015
Accepted date: 22 December 2015

Please cite this article as: Schobben, Martin, Ullmann, Clemens Vinzenz, Leda, Lucyna, Korn, Dieter, Struck, Ulrich, Reimold, Wolf Uwe, Ghaderi, Abbas, Algeo, Thomas J., Korte, Christoph, Discerning primary versus diagenetic signals in carbonate carbon and oxygen isotope records: An example from the Permian–Triassic boundary of Iran, *Chemical Geology* (2015), doi: 10.1016/j.chemgeo.2015.12.013

Discerning primary versus diagenetic signals in carbonate carbon and oxygen isotope records:

An example from the Permian-Triassic boundary of Iran

Martin Schobben[a,*], Clemens Vinzenz Ullmann[b,c], Lucyna Leda[a], Dieter Korn[a], Ulrich Struck[a], Wolf Uwe Reimold[a,d], Abbas Ghaderi[e], Thomas J. Algeo[f,g], Christoph Korte[b]

[a] Museum für Naturkunde, Leibniz-Institut für Evolutions- und Biodiversitätsforschung, Invalidenstr 43, D-10115 Berlin, Germany

[b] Department of Geosciences and Natural Resource Management, University of Copenhagen, ØsterVoldgade 10, DK-1350, Copenhagen, Denmark

[c] University of Exeter, Camborne School of Mines, College of Engineering, Mathematics and Physical Sciences, Penryn Campus, Penryn, Cornwall TR10 9FE, UK

[d] Humboldt Universität zu Berlin, Unter den Linden 6, 10099 Berlin, Germany

[e] Department of Geology, Faculty of Sciences, Ferdowsi University of Mashhad, Azadi Square, 9177948974 Mashhad, Iran

[f] Department of Geology, University of Cincinnati, Cincinnati, OH 45221-0013, U.S.A.

[g] State Key Laboratories of BGEG and GPMR, China University of Geosciences, Wuhan 430074 P.R. China

ARTICLE INFO

Keywords: diagenesis; trace elements; chemostratigraphy; authigenic carbonates; biogeochemical carbon cycle

ABSTRACT

Sedimentary successions across the Permian-Triassic boundary (PTB) are marked by a prominent negative carbon isotope excursion. This excursion, found in both fossil (e.g., brachiopod) and bulk carbonate at many sites around the world, is generally considered to be related to a global carbon cycle perturbation. Oxygen isotopes also show a negative excursion across the PTB, but because $\delta^{18}O$ is more prone to diagenetic overprint (especially in bulk carbonate), these data are often not used in palaeoenvironmental analyses. In the present study, bulk-rock and brachiopod $\delta^{13}C$ and $\delta^{18}O$, as well as conodont $\delta^{18}O$, were analyzed in PTB successions at Kuh-e-Ali Bashi and Zal (NW Iran) in order to evaluate diagenetic overprints on primary marine isotopic signals. The results show that the use of paired C-O isotopes and Mn-Sr concentrations is not sufficient to identify diagenetic alteration in bulk materials, because $\delta^{13}C$-$\delta^{18}O$ covariation can be due to environmental factors rather than diagenesis, and Sr/Ca and Mn/Ca ratios can vary as a function of bulk-rock lithology. Comparison of $\delta^{13}C$ profiles shows that all bulk carbonate is altered to some degree, although the general bulk-rock trend mimics that of the brachiopod data with a systematic offset of –1.2(±0.4)‰. This suggests that the first-order $\delta^{13}C$ trend in bulk carbonate is generally robust but that the significance of small-scale carbon isotope fluctuations is uncertain, especially when such fluctuations are linked to lithologic variation. The PTB interval, which is marked by a low-carbonate 'Boundary Clay' in the study sections, may be especially prone to diagenetic alteration, e.g., via late-stage dolomitization. Comparison of oxygen-isotope profiles for bulk rock and well-preserved fossils (both brachiopods and conodonts) shows that the former are offset by –2.1(±0.4)‰. Diagenetic modeling suggests that these offsets were the product mainly of early diagenesis at burial temperatures of ~50-80°C and water/rock ratios of <10. Authigenic carbonates precipitated during early diagenesis represent a potentially major sink for isotopically light carbon -- at a global scale - that has received relatively little attention to date.

1. Introduction

Bulk-carbonate isotope data have been widely employed as a proxy for seawater chemistry, climate, and marine productivity during the Proterozoic (Kaufman and Knoll, 1995; Knauth and Kennedy, 2009; Knoll et al., 1986), Palaeozoic (Baud et al., 1989; Buggisch and Joachimski, 2006; Holser and Magaritz, 1987; Marshall and Middleton, 1990; Saltzman, 2002), and Mesozoic (Jenkyns and Clayton, 1986; Schlanger et al., 1987). Similarly to biogenic low-Mg calcite (e.g., brachiopods and belemnites), carbon isotope ratios of marine bulk carbonate have been assumed to be a faithful proxy for the $\delta^{13}C$ of dissolved inorganic carbon (DIC) in palaeoseawater (Buggisch and Joachimski, 2006; Holser and Magaritz, 1987; Payne et al., 2004), and C-isotopic excursions are regarded as robust stratigraphic correlation markers (Hermann et al., 2010; Korte and Kozur, 2010; Kraus et al., 2009).

Palaeoclimatic studies utilizing oxygen isotope palaeothermometry generally prefer the use of low-Mg carbonate shells, because they are thought to be less susceptible to diagenetic resetting than other carbonate phases (Brand, 1989; Korte et al., 2005a, 2005b; Mii et al., 1999; van Geldern et al., 2006; Veizer et al., 1999). On the other hand, bulk-carbonate oxygen isotope compositions are usually rejected as a climate proxy owing to their susceptibility to diagenetic alteration. This susceptibility is due to the large size of the oxygen reservoir in diagenetic fluids and the greater isotope fractionation effects associated with oxygen (relative to carbon) (Brand and Veizer, 1981; Marshall, 1992). Bulk-rock isotope records, however, can be generated with high temporal resolution and do not depend on the availability of shelly fossils, which are often absent during phases of severe environmental stress, such as mass extinction events. Thus, in many cases there are distinct advantages to working with bulk-carbonate C and O isotope records.

Different opinions exist regarding the reliability of bulk-carbonate samples as a recorder of primary palaeoseawater isotopic signals (see discussion in Brand et al., 2012a). It has been suggested that abrupt stratigraphic shifts in bulk-carbonate $\delta^{13}C$ associated with lithological breaks should be treated as possible evidence of stratigraphic gaps and/or diagenetic alteration of the host

rock (Algeo, 1996; Marshall, 1992). Carbonate sediments are complex recorders of isotopic information because they consist of multiple components, each potentially having a different initial C-O isotopic composition, and each responding in a unique manner to a series of diagenetic events leading to final stabilization in the burial environment (Brand et al., 2012b; Jenkyns and Clayton, 1986). An improved understanding of how diagenesis affects the isotopic composition of carbonate sediments is needed in order to better isolate the primary versus secondary components of bulk-rock $\delta^{13}C$ and $\delta^{18}O$ signatures.

Various sedimentological, textural, and chemical indicators have been used to evaluate diagenetic influences on bulk-carbonate isotope chemistry (Al-Aasm and Veizer, 1986; Brand and Veizer, 1980; Melim et al., 2002). Textural changes, such as cementation and recrystallization features, can give a general idea about the diagenetic history of a sample, but they are often insufficient for detailed reconstructions, as too little is known about the timing and physical conditions of their development (Melim et al., 2002; Munnecke et al., 1997). Chemical indicators of diagenetic alteration, such as Sr and Mn concentrations, have been widely used (Banner and Hanson, 1990; Brand and Veizer, 1980; Middelburg et al., 1987; Pingitore, 1978; Pingitore et al., 1988). However, many carbonate units have experienced multiple diagenetic regimes and fluids with spatially and temporally variable chemical properties, making accurate quantification of these processes difficult.

We have undertaken a comparative fossil and bulk-rock geochemical investigation from outcrop samples of two P-Tr boundary sections (Kuh-e-Ali Bashi and Zal) in NW Iran with the goal of assessing bulk-carbonate carbon-oxygen isotopic records as a proxy for primary marine carbonate isotopic composition. We analysed the C-O isotopic composition of brachiopods that were well-preserved (as determined by micropetrographic and elemental analyses in Schobben et al., 2014), in addition to making use of conodont O isotope data from earlier studies, as proxies for primary marine carbonate isotopic compositions, and we compared these results with bulk-carbonate $\delta^{13}C$ and $\delta^{18}O$. We have then assessed the degree of diagenetic alteration of bulk

carbonate based on minor-element concentrations (i.e., Mn/Ca, Sr/Ca, and Mg/Ca). Our data provide insight into the degree of secondary overprinting of the primary marine carbonate isotopic signals of the study units. The implications of these results extend beyond the present study sections, however, providing a new approach for analysis of diagenetic effects and recovery of primary marine carbonate isotopic signals in bulk-carbonate samples of any age.

2. Study locales

The Kuh-e-Ali Bashi 1 (as defined by Teichert et al., 1973), at 38.940°N, 45.520°E, and Zal, at 38.733°N, 45.580°E, sections of the Julfa region of NW Iran (Fig. 1A) are located on the north-northeastern margin of the Northwestern Iranian Terrane, which belonged to the Cimmerian microcontinents during the latest Permian (Fig. 1B). In this area, carbonate rock successions spanning the P-Tr boundary interval consist of three major lithological units (in stratigraphic order): the *Paratirolites* Limestone (which is the upper part of the Ali Bashi Formation), the 'Boundary Clay'(Aras Member as defined by Ghaderi et al., 2014), and the '*Claraia* Beds' (the latter two forming the Elikah Formation).

The red nodular *Paratirolites* Limestone beds have $CaCO_3$ contents between 70 and 90 wt. % (Ghaderi et al., 2014; Leda et al., 2014), classifying them as argillaceous limestone. The limestone beds are separated by shale horizons with a thickness of not more than 10 cm and usually less than 5 cm, and which become thinner towards the top of the *Paratirolites* Limestone. The individual limestone nodules have a partly rounded surface and show a micritic matrix of generally similar composition. The rare macrofossil assemblages comprise ammonites, nautiloids, rugose corals, fish remains, and brachiopod shells. Microfossils are strikingly abundant in the insoluble residue of acid digestions, yielding pectinoform and platform elements from conodonts and actinopterygian teeth. Calcareous green algae and radiolarians have been identified from thin sections (Leda et al., 2014). Other features of the *Paratirolites* Limestone are carbonate nodules

coated with Fe-Mn crusts, and Fe-Mn coatings of discontinuity surfaces accompanied by biogenic encrustations (Leda et al., 2014; Mohtat Aghai et al., 2011; Fig. 2B). Besides micrite, the matrix contains some minor sparry cement and in-situ crystallization (neomorphic spar). The nodular limestones with hardground features and the pelagic fauna likely signify low rates of carbonate accumulation in a deep-shelf environment (~100-200 m) (Leda et al., 2014).

The Boundary Clay, common in most of the Iranian P-Tr sections (Ghaderi et al., 2014; Heydari et al., 2003; Leda et al., 2014; Taraz, 1971), overlies the *Paratirolites* Limestone, and its base marks the end-Permian mass extinction (EPME) horizon (Kozur, 2007). The lithology can be classified as red claystone and red/green marl. It reaches thicknesses of 1.2 m at Kuh-e-Ali Bashi and 0.6 m at Zal, where it contains 18 and 35 wt. % $CaCO_3$, respectively (Ghaderi et al., 2014). Skeletal components are less abundant than in the *Paratirolites* Limestone but ostracod, bellerophontid gastropod, and sponge remains occur frequently (Fig. 2E). The marine benthos points to a continuation of fully marine conditions during deposition of this unit. The siliciclastic matrix contains microcrystalline spar and micrite and is intersected by abundant anastomosing stylolites.

In the overlying '*Claraia* Beds', only the lower 5 to 10 m were studied here. The base of this unit is slightly below the conodont-defined P-Tr boundary (Ghaderi et al., 2014; Kozur, 2007). At Kuh-e-Ali Bashi, the lower part (1.10 m) of the '*Claraia* Beds' is lithologically similar to the pre-extinction *Paratirolites* Limestone, consisting of argillaceous nodular limestone with intercalated marl beds. At Zal and above 1.10 m in the Kuh-e-Ali Bashi section, the '*Claraia* Beds' consist of grey, thick-bedded, platy limestone. Leda et al. (2014) recognised that these limestones exhibit a recrystallized texture, relating to microspar cementation and in-situ recrystallization (Fig. 2C). These lithologies were deposited in a low-energy environment and represent a continuation of deep-water conditions from the Upper Permian (Leda et al., 2014).

The two sections have been well-studied with respect to their biostratigraphy and sedimentology (Ghaderi et al., 2014; Korte and Kozur, 2005; Kozur, 2007; Leda et al., 2014;

Stepanov et al., 1969; Teichert et al., 1973). They both contain the Boundary Clay with the EPME horizon at its base. These P-Tr boundary sections differ from coeval sites in Japan, China, and Turkey, all of which show erosional truncation of end-Permian strata possibly caused by submarine dissolution (Payne et al., 2007) or subaerial exposure (Collin et al., 2009).

Local diagenetic alteration, implied by lithological and facies changes, has been put forward as an explanation for observed short-term $\delta^{13}C$ trends confined to the Boundary Clay of some Iranian P-Tr sections (Heydari et al., 2001, 2003; Korte et al., 2004a, 2004b; Korte and Kozur, 2005). It has been suggested that calcareous clays, such as those found in the Boundary Clay, are susceptible to post-depositional recrystallization that may alter their carbonate $\delta^{13}C$ composition (Knauth and Kennedy, 2009).

3. Methods

Aliquots of the samples for isotope analysis were taken from fresh surfaces of carbonate rocks, using a micro drill. Late-diagenetic cracks, veins, and stylolites were rejected to avoid major contamination of the samples. Larger sample splits (one gram) for elemental analysis were taken by trimming off altered parts of hand samples using a trim saw and crushing the residual with the aid of a mechanical agate mill. The material sampled by micro-drill and by crushing of hand samples, thus, consisted of a similar mixture of allochems, micrite, and early diagenetic cements, the relative proportions of which could not be discerned through visual inspection. The generated aliquots of such sampling procedures are commonly referred to as ‘micritic carbonate’ or ‘lithographic limestone’ (cf. Brand et al. 2012a, 2012b) and will be referred to as either ‘bulk-rock’ or ‘whole-rock’ samples in the following.

Stable isotope measurements were carried out using a Thermo FinniganGasbench II linked online to a THERMO/Finnigan MAT V isotope ratio mass spectrometer in the stable isotope laboratory of the Museum für Naturkunde in Berlin. After flushing the reaction vessels (12 ml

borosilicate glass capped with a rubber septum LABCO) with helium, approximately 30 µl of anhydrous phosphoric acid was injected through the septum into the sealed reaction vessel by using a disposable syringe. The sample was ready for isotope measurement after approximately 1.5 hours of reaction time at 72°C. Reference gas was pure CO_2 (99.995 %) from a cylinder calibrated against the IAEA reference materials (NBS 18, NBS 19). The accuracy of both $\delta^{13}C$ and $\delta^{18}O$ was determined against an in-house standard (Pfeil STD; Solenhofen Limestone) and the precision determined by repeated measurements was generally better than ±0.1 ‰ (1σ). Oxygen and carbon isotopes are reported relative to Vienna Pee Dee Belemnite (VPDB) in standard delta notation.

One-gram splits of ground material were used for elemental analysis of the acid-soluble part (see the Supplementary Text, Supplementary Figure 1 and Supplementary Table 1 for additional discussion on the data generated by this procedure). Acid digestion was carried out using 20 ml 0.33 M acetic acid over 48 hours, with the solution constantly being agitated. The insoluble and soluble fractions were separated by filtration using a cellulose-nitrate membrane (0.45 µm) and were then dried and weighed. A part of the soluble fraction was dissolved with 0.2 M nitric acid in order to obtain a matrix-matched solution for analysis by Inductively Coupled Plasma - Optical Emission Spectrometry (ICP-OES) carried out at the University of Copenhagen (see Ullmann et al., 2013a for methodology). The Ca concentration of the solution was approximated; this allowed for a matrix match of the 0.2 M HNO_3 blank solution and multi-element reference solutions fabricated for a three-point calibration. The precision was monitored by international standards JDo-1 and JLs-1 yielding accuracies for Sr/Ca, Mn/Ca and Mg/Ca ratios with averages better than 5 % and reproducibility with biases less than 10% (2σ) (Table 1) (Imai et al., 1996). Calcite ($CaCO_3$) concentrations of the samples were determined by the weight loss-acid digestion method by using a 2M HCl solution (e.g., Siesser and Rogers, 1971). A small subset of the decalcified samples of the *Paratirolites* Limestone Member were analyzed for concentrations and carbon isotope compositions of the organic fraction with a THERMO/Finnigan MAT V isotope ratio mass spectrometer, coupled to a THERMO Flash EA 1112 elemental analyzer via a THERMO/Finnigan Conflo IV interface, in

the stable isotope laboratory of the Museum für Naturkunde, Berlin. Organic carbon isotope measurements were converted to the VPDB scale by reference to the IAEA standard CH3. Standard deviations for repeated isotope measurements of lab standard material (peptone) were generally better than ±0.1 per mille (‰). The program R and the packages gridExtra, gTable and ggplot2 have been used for graphical plots and statistics (http://cran.r-project.org/).

4. Results

4.1. Isotope results

The $\delta^{13}C$ of carbonate rocks from Kuh-e-Ali Bashi and Zal (including data of Schobben et al., 2014) range from –2.8 to 3.5 ‰ and from –0.9 to 3.4 ‰, respectively (Fig. 3, Supplementary Tables 2 and 3). A general decline in bulk-carbonate $\delta^{13}C$ occurs upsection for samples from both localities, starting within the *Clarkina bachmanni* Zone. The pre-extinction brachiopod $\delta^{13}C$ values are slightly heavier but follow the general bulk-rock trend (Fig. 3). No articulated brachiopods are present in the post-extinction interval. The Kuh-e-Ali Bashi section is marked by two bulk-rock $\delta^{13}C$ minima of –1.4 and –0.7 ‰ at 1.70 m and 0.71 m below the EPME horizon, respectively. An inflection to even lower bulk-rock values marks the base of the Boundary Clay. However, this pattern is not observed at Zal, where bulk-rock $\delta^{13}C$ fluctuates around 1.5 ‰ in the correlative interval. Parallel bulk-rock $\delta^{13}C$ minima are observed at both sites within the *Hindeodus parvus* Zone. In this interval, the carbon isotope values average ca. –3.0 and –0.1 ‰ for Kuh-e-Ali Bashi and Zal, respectively, with a single sample in the latter section yielding a lower $\delta^{13}C$ value (–0.9 ‰ at +2.0 m). Post-extinction bulk-rock $\delta^{13}C$ of both sections remains more depleted than in pre-extinction strata, with values around –1 ‰. At Kuh-e-Ali Bashi, one additional negative $\delta^{13}C$ excursion (–1.4 ‰) occurs at 3.50 m above the EPME horizon.

The $\delta^{18}O$ of carbonate rocks from Kuh-e-Ali Bashi and Zal (including data of Schobben et al., 2014) range from –8.1 to –4.0 ‰ and from –8.3 to –3.0 ‰, respectively (Fig. 3, Supplementary

Tables 2 and 3). The bulk-rock oxygen isotope values from the lower *Paratirolites* Limestone of both sections are ca. –5.0 ‰ (Fig. 3). At the base of the Boundary Clay, bulk-rock $\delta^{18}O$ declines to ca. –7.0 to –8.0 ‰ and remains more depleted (ca. –7.0 ‰) upsection compared to pre-extinction strata. Calcite brachiopod shell $\delta^{18}O$, taken from Schobben et al. (2014), are heavier than coeval bulk-rock data (–4.0 and –3.0 ‰ VPDB). Conodont $\delta^{18}O$ is normally reported on the SMOW scale, but here we translate these data to the VPDB scale to simplify carbonate/apatite $\delta^{18}O$ comparisons. However, this comparison is not straightforward owing to the varying temperature dependence of equilibrium fractionations between water and solid phases (Wenzel et al., 2000). We used two different approaches for translating conodont $\delta^{18}O$ (also taken from Schobben et al., 2014) to the VPDB-scale: (1) by comparing the offset between pristine brachiopod and conodont oxygen isotope data, and (2) by back-calculating conodont $\delta^{18}O$ derived palaeotemperatures (as given in Schobben et al., 2014) using a carbonate-water fractionation equation from Kim and O'Neil (1997). Comparing the VPDB-translated conodont $\delta^{18}O$ derived from these two methods reveals a discrepancy of up to 0.5 ‰ (cf. Wenzel et al., 2000). This uncertainty is given as error bars on the VPDB scale in Figure 3. Pre-extinction conodont $\delta^{18}O$ ranges between equivalents of –4.0 and –3.0 ‰ VPDB with an uncertainty of about 0.5 ‰. Post-extinction conodont $\delta^{18}O$ values correspond to calcite values of ca. –5.0 ‰ VPDB (uncertainty ~0.3 ‰). and thus more depleted.

The total organic carbon (TOC) obtained from the *Paratirolites* Limestone unit ranges from 0.01 to 0.02 %, with organic carbon $\delta^{13}C$ values of –25.4 to –23.2 ‰ (VPDB).

4.2. Elemental ratios

Mn/Ca – At Kuh-e-Ali Bashi, the *Paratirolites* Limestone has relatively stable Mn/Ca ratios averaging at about 1.8 mmol/mol ($1\sigma = 0.6$, $n = 25$) for the calcite fraction (Fig. 3, Supplementary Tables 2 and 3). A prominent peak of 11.9 mmol/mol occurs within the Boundary Clay followed by a steady decrease up-section, but Mn/Ca remains higher than average pre-extinction values (median

of 2.7 mmol/mol; 1σ = 0.6, n = 24) up to a height of 2.35 m above the base of the EPME horizon. The lowest values at Kuh-e-Ali Bashi are recorded for the upper part of the Elikah Formation, yielding a median of 1.1 mmol/mol (1σ = 0.4, n = 9). At Zal, the *Paratirolites* Limestone is marked by Mn/Ca ratios of 1.6 mmol/mol (median; 1σ = 0.1, n = 4) (Fig. 3, Supplementary Tables 2 and 3). Similar to Kuh-e-Ali Bashi, the Zal section displays a marked positive excursion with a Mn/Ca maximum of 5.3 mmol/mol within the Boundary Clay (median = 2.6 mmol/mol; 1σ =1.8, n= 10). Elevated Mn/Ca ratios between 1.1 and 3.3 mmol/mol occur within the interval up to 2.00 m above the EPME horizon. The upper part of the Elikah Formation has Mn/Ca ratios of 0.6 to 0.7 mmol/mol (n = 10), and these are the lowest ratios within the section.

Sr/Ca – At Kuh-e-Ali Bashi, the Sr/Ca ratios are uniform throughout the *Paratirolites* Limestone with a median of 0.6 mmol/mol (1σ = 0, n = 25) (Fig. 3, Supplementary Tables 2 and 3). From the base of the Boundary Clay to 2.00 m above, the Sr/Ca ratios are marked by some small fluctuations with a median value of 0.5 mmol/mol (1σ = 0.1, n = 23). The Sr/Ca ratios display an increase up to 0.9 mmol/mol in the Elikah Formation, with a sharp positive excursion reaching 1.7 mmol/mol at 3.07 m above the EPME horizon. At Zal, the Sr/Ca ratios of the *Paratirolites* Limestone yield a median of 0.7 mmol/mol (1σ = 0.1, n = 4) (Fig. 3, and Supplementary Tables 2 and 3) with a peak of 1.4 mmol/mol for the Boundary Clay. At 2.00 meters above the EPME horizon, the Sr/Ca ratio displays large fluctuations with maxima of 2.3, 2.6, 3.1 and 3.5 mmol/mol.

Mg/Ca – The Mg/Ca values at Kuh-e-Ali Bashi and Zal are relatively stable throughout the study interval with a median of 17.5 mmol/mol (1σ = 4.9, n = 57) and 21.4 mmol/mol (1σ = 7.1, n = 17), respectively. Distinctly higher Mg/Ca ratios occur in the Boundary Clay, reaching 590 and 420 mmol/mol at Kuh-e-Ali Bashi and Zal, respectively (Figs. 3, Supplementary Tables 2 and 3).

5. Screening for diagenesis

5.1. Recognition of diagenetic signals in carbonate $\delta^{13}C$-$\delta^{18}O$ records

Multiple methods have been developed for assessing diagenetic influences on carbonate $\delta^{13}C$ and $\delta^{18}O$ records. Partial diagenetic alteration of marine carbonate sequences is likely to result in covariation of carbon and oxygen isotope ratios of bulk carbonate (e.g., Brand and Veizer, 1981). Bulk-rock $\delta^{13}C$ values are, therefore, often screened by quantifying their correlation with $\delta^{18}O$ using Pearson's r correlation coefficients (e.g., Heydari et al., 2001). Our data show a highly significant positive correlation between $\delta^{13}C$ and $\delta^{18}O$ (p-value < 0.001; Table 2). This pattern is thought to be diagnostic for lithification of carbonate rocks under the influence of meteoric water or in phreatic lenses (Brand and Veizer, 1981). However, such an interpretation might be too simplistic because our samples are positioned in a region of the $\delta^{13}C$-$\delta^{18}O$ cross-plot (Fig. 4B) that is not typical for carbonate rock lithified in contact with meteoric or phreatic water (cf. Knauth and Kennedy, 2009). In addition, the overlying >100 m of Triassic sediments show no indications of subaerial exposure (Horacek et al., 2007; Leda et al. 2014; Richoz et al., 2010). Both observations provide evidence against the interpretation that meteoric diagenesis has altered the C-O isotope values of the study successions. Correlations between $\delta^{13}C$ and $\delta^{18}O$ do not necessarily represent secondary diagenetic signals (Marshall, 1992; Ullmann and Korte, 2015). Severe environmental perturbations associated with climate warming (hence more negative $\delta^{18}O$) and a concurrent negative $\delta^{13}C$ excursion are known from the Paleocene-Eocene Thermal Maximum (PETM; Zachos et al., 2006) and the Early Toarcian Oceanic Anoxic Event (T-OAE, Hermoso et al., 2012; Ullmann et al., 2014), and this is probably also the case for the P-Tr boundary. The resulting unidirectional, environmentally controlled signal on both isotope systems resembles meteoric diagenesis and makes any inferences about sample preservation from a $\delta^{13}C$-$\delta^{18}O$ cross-plot ambiguous.

Elemental data, especially Mn and Sr, are also widely utilized to identify diagenetic alteration in bulk-rock samples (Brand et al., 2012a, 2012b; Denison et al., 1994). Manganese usually becomes enriched during post-depositional dissolution and recrystallization of carbonate (Brand and Veizer, 1980; Denison et al., 1994; Pingitore, 1978;), and strontium – modulated by its variable initial concentration in primary carbonate phases (Korte and Hesselbo, 2011; Ullmann et

al., 2013b) – is lost due to dissolution and recrystallization of diagenetic calcite phases (Brand and Veizer, 1980; Veizer et al., 1971). Rather than showing strong correlations with the C and O isotopic proxies, Mn/Ca and Sr/Ca ratios follow smooth trends in the Kuh-e-Ali Bashi and Zal sections where data density is sufficient (e.g., in the Boundary Clay interval; Fig. 3). Lithologically-driven variation is evident at the transitions from nodular limestone (mainly the *Paratirolites* Limestone) to clay (the Boundary Clay) and to platy limestone (mainly the '*Claraia* Beds' Fig. 5). The inference of strong lithologic control on Mn/Ca and Sr/Ca is further demonstrated by a Kruskal-Wallis rank sum test suggesting significant differences between lithologies (p-value <0.001). This coupling of Sr/Ca and Mn/Ca to lithology rather than to the isotopic trends (Figs. 4 C and D) precludes an assessment of carbonate preservation based on these elemental ratios beyond the choice of arbitrary threshold values, whose application would bias further discussion of the data.

Mg/Ca ratios in carbonate samples can help to distinguish between diagenetic endmembers of low-Mg calcite and dolomite (e.g., Brand and Veizer, 1980). Several carbonate samples in the Boundary Clay interval of Kuh-e-Ali Bashi and Zal show Mg enrichments beyond the limit of low-Mg calcite, Mg enrichment being ten times greater than for the clastic fraction. The high Mg/Ca content, together with the occurrence of rhombic crystals of dolomite in this interval, suggests a localized process of dolomitization (Figs. 2D and 3; cf. Leda et al., 2014). A burial diagenetic process that might be tied to a Mg-enriched diagenetic fluid is the transformation of smectite to illite (McHargue and Price, 1982; Sternbach and Friedman, 1986). Samples enriched in Mg show a tendency toward heavier carbon and oxygen isotope values than associated low-Mg calcite samples (cf. Brand et al., 2012a,b). A similar relationship between dolomitization and more positive $\delta^{13}C$ values for time-equivalent beds in Meishan, China (Bed 27) has also been pointed out by Xie and Wang (2011). From a bulk-rock perspective, Mg/Ca ratios are the only elemental proxy data in the study sections that can be tied to a post-depositional effect on carbon and oxygen isotope ratios.

Besides textural and lithological examination (Al-Aasm and Veizer, 1986), preservation of brachiopod shell calcite is often evaluated using Mn and Sr concentrations (Brand et al., 2012a;

Korte et al., 2005a, 2005b; Mii et al., 1999; van Geldern et al., 2006). Brachiopod samples from Kuh-e-Ali Bashi show Mn/Ca ratios of 0.36 mmol/mol or lower, Sr/Ca ratios of 0.35 to 0.59 mmol/mol, and good preservation of shell microstructure (Schobben et al., 2014). The observed Mn/Ca ratios are within the limits of those generally accepted as indicative of good brachiopod shell preservation (Korte et al., 2003; Fig. 4A). Measured Sr/Ca ratios, however, are similar or slightly lower than the lowest values observed in modern brachiopods (Brand et al., 2003), which could be interpreted as a sign of diagenesis that generally causes Sr/Ca in biogenic calcite to decrease (e.g. Al-Aasm and Veizer, 1986; Brand and Veizer, 1980; Ullmann and Korte, 2015). However, the seawater Sr/Ca ratio, which exerts a first-order control on shell Sr/Ca, has changed significantly through time and is predicted to have been low during times of 'aragonite seas' (Steuber and Veizer, 2002, Ullmann et al., 2013b). Average observed Permian brachiopod Sr/Ca ratios are indeed lower than their modern counterparts (Steuber and Veizer, 2002), so that the observed geochemical composition of the Kuh-e-Ali Bashi brachiopods is plausible for well-preserved Permian brachiopods. Kuh-e-Ali Bashi brachiopod calcite is, therefore, interpreted to reflect a near-primary marine signal (see also Schobben et al., 2014).

5.2. *Evaluation of primary and diagenetic influences on $\delta^{13}C$ profiles of Iranian PTB sections*

The bulk-carbonate carbon isotope curves do not deviate substantially from earlier records for the same sections (e.g., Korte et al., 2004c; Korte and Kozur, 2005; Richoz et al., 2010; Fig. 6): A negative trend through the Permian-Triassic boundary interval is clearly visible (e.g., Baud et al., 1989; Hermann et al., 2010; Korte et al., 2004a; Korte and Kozur, 2010; Tong et al., 2007), resembling the results from coeval deep-water PTB sections containing the Boundary Clay (Abadeh and Meishan) and shallow-water sections that lack the Boundary Clay (e.g., Nhi Tao, Pufels, and Gartnerkofel) (Korte and Kozur, 2010; Fig. 6).

Carbon isotope data reveal a relatively stable offset between brachiopods and bulk-rock samples ($\Delta^{13}C_{bio\text{-}bulk}$) of ~1.2 ‰ (±0.4 ‰), based on comparison of the smoothed curves from Figure 7. The smoothed curves, which were generated using polynomial kernel regression, are necessary for data interpolation, as much of the brachiopod and whole-rock data do not come from matching stratigraphic levels. The uniformly positive $\Delta^{13}C_{bio\text{-}bulk}$ likely reflects pervasive weak alteration of bulk-rock $\delta^{13}C$ (cf. Brand et al., 2012b), as there is no evidence for a general primary ^{13}C-enrichment in brachiopods compared to other carbonate components (Wefer and Berger, 1991).

A source of ^{13}C-depleted carbon is oxidation of sedimentary organic matter. Aerobic respiration of organic carbon (OC) generates CO_2 that can lead to carbonate dissolution on a 1:1 molar basis, generating bicarbonate (HCO_3^-) that is markedly ^{13}C-depleted. Incorporation of such isotopically light carbon during precipitation of secondary carbonate phases causes a negative shift in bulk-rock $\delta^{13}C$. The amount of OC required to produce the observed $\Delta^{13}C_{bio\text{-}bulk}$ (Fig. 7) can be computed by the following equation:

$$OC = \left(\frac{\Delta^{13}C_{bio-bulk}}{\delta^{13}C_{bulk} - \delta^{13}C_{HCO_3} - \delta^{13}C_{dia}} \right) Fc \qquad (1)$$

where $\delta^{13}C_{HCO_3}$ and $\delta^{13}C_{dia}$ stand for the carbon isotope composition of pore water bicarbonate and diagenetic carbonate precipitates, respectively. The fraction of carbon present in calcium carbonate is given as Fc (= 0.12, i.e., 12.0 amu/100.1 amu). The isotopic composition of the diagenetic carbonate fraction depends, in turn, on $\delta^{13}C_{HCO_3}$ and temperature, and it can be calculated according to the relationship of Emrich et al. (1970). A $\delta^{13}C_{HCO_3}$ of –13.0 ‰ is reasonable, when considering measured $\delta^{13}C_{org}$ of –25.4 to –23.2 ‰ mixed with seawater bicarbonate having an average isotopic value of ~0.0 ‰ and following the stoichiometry of aerobic metabolism-driven carbonate dissolution. Following this approach, the observed $\Delta^{13}C_{bio\text{-}bulk}$ can be explained by authigenic carbonate incorporation from sediments with an initial OC value of ~1.0 %. This estimate is in good agreement with the inferred original sedimentary OC concentration (0.50-0.90 %) of the study

samples, when applying the back-calculation procedure of Algeo et al. (2013) to the measured TOC concentrations (0.01-0.02 %). Following this procedure, TOC values are first converted to organic carbon accumulation rates (OCAR), based upon bulk accumulation rates (BAR). The nodular nature of this stratigraphic interval (the *Paratirolites* Limestone unit) has been attributed to a restricted sediment supply, and sedimentation rates (SR) would likely not have exceeded 0.5 cm kyr^{-1} (Leda et al., 2013; Richoz et al., 2010). The OCAR can be derived from TOC, SR and the density (ρ) for bulk carbonate rock, per Equation 2, taken from Algeo et al. (2013):

$$OCAR = TOC \times \rho \times SR \quad (2)$$

where, an average ρ of 2.5 g m^{-2} yr^{-1} has been used. Thermal loss of OC can be estimated from vitrinite reflectance values (R_0), which are ~0.65, for the NW Iranian localities. OC loss due to metamorphism is given by Equation 3, taken from Algeo et al. (2013):

$$\log(OCAR / OCAR' = -0.283 R_0 \quad (3)$$

where $OCAR'$ stands for the pre-metamorphosed OC content. Long exposure to oxygenated conditions, as a result of low SR, would have resulted in a (near total) aerobic degradation of the available sedimentary OC. Subsequent microbial sulfate reduction (MSR), an important contributor to sedimentary OC oxidation, likely had a minimal impact on the remaining OC, based on chromium-reducible sulfur concentrations (S_{pyr}) of 10 ppm (Schobben et al., 2015). Both loss of OC by MSR and oxic degradation can be quantified by successive application of Equations 4 and 5, respectively, as given in Algeo et al. (2013):

$$OCAR'' = OCAR' + (0.75 S_{pyr} BAR) \quad (4)$$

$$OCAR''' = OCAR'' 10^{0.51(3.1 - BAR)} \quad (5)$$

Here, $OCAR''$ and $OCAR'''$ stand for the organic matter accumulation before MSR and oxic degradation, respectively. The original OC value of the sediment (before the start of early diagenesis) can be derived by dividing $OCAR'''$ with BAR. The back-calculated original OC values

of the study samples suggest that the process of OC oxidation and related carbonate dissolution can account for the observed offset between brachiopod and whole-rock $\delta^{13}C$. Although this large extrapolation (> ×10) of measured TOC to obtain the original sedimentary OC values is connected with a large uncertainty (see Algeo et al., 2013), the computed values are consistent with OC for open-ocean carbonate platform sediments (~1.0 %) based on modern observations (Emerson and Hedges, 2003).

5.3. Evaluation of primary and diagenetic influences on $\delta^{18}O$ profiles of Iranian PTB sections

The oxygen isotopic composition of the phosphate in conodont apatite has proven valuable for palaeoclimatic reconstructions of the latest Permian and Early Triassic (Joachimski et al., 2012; Romano et al., 2013; Schobben et al., 2014; Sun et al., 2012). Our O-isotope record of Iranian conodonts through the Permian-Triassic boundary interval is constructed from conodont platform elements with colour alteration indices (CAI) between 1.0 and 1.5, indicating minor thermal overprints (Schobben et al., 2014). This oxygen isotope record shows stable values throughout the latest Permian, which is also the case for the latest Permian brachiopod O-isotope record (Fig. 3). The general agreement between the conodont and brachiopod isotope records constitutes an additional argument for good fossil preservation in the study sections. These fossil records can, therefore, be taken as a baseline for assessing diagenetic alteration of the bulk-rock O-isotope record (e.g., Brand et al., 2012a, 2012b). Brachiopods inform about the carbon and oxygen isotope evolution of the latest Permian, before they disappear at the EPME horizon at the base of the Boundary Clay (Fig. 3). For the remainder of the study succession, only conodont phosphate is available for comparison with bulk-rock data.

Despite some uncertainty concerning the conodont $\delta^{18}O$ correction factor (see Section 4.1), a significant offset (median: 2.1 ‰ ± 0.4 ‰) exists between conodont/brachiopod and bulk-carbonate $\delta^{18}O$ ($\Delta^{18}O_{bio\text{-}bulk}$) (Fig. 7). Thus, the bulk-rock $\delta^{18}O$ values almost certainly have been

shifted by diagenetic processes, with higher burial temperatures during recrystallization leading to reduced fluid-solid fractionation and, thus, more negative $\delta^{18}O$ values for secondary carbonate phases (cf. Algeo et al., 1992). The fraction of recrystallized carbonate rock that equilibrated with the diagenetic fluid ($F_{CaCO_3(au)}$) would determine the final whole-rock $\delta^{18}O$ and is linked to burial temperature and the oxygen isotope composition of the diagenetic fluid via Equation 6:

$$F_{CaCO_3(au)} = \frac{\Delta^{18}O_{bio-bulk}}{\delta^{18}O_{bio} - \delta^{18}O_{dia}} \quad (6)$$

where the $\delta^{18}O_{bio}$ and $\delta^{18}O_{bulk}$ is taken as the median of measured conodont/brachiopod (combined) and whole-rock oxygen isotope values, respectively. The oxygen isotope composition of the diagenetic carbonate ($\delta^{18}O_{dia}$), which depends on the isotope value of the pore water and the temperature at which secondary precipitation occurred, can be calculated using the fractionation relationship of Kim and O'Neil (1997). The study sites experienced maximum burial temperatures of 80 °C, based on low conodont CAI (1.0-1.5). The $\delta^{18}O_{fluid}$ was probably between that of contemporaneous seawater (ca. –1.0 ‰) and a pore fluid equilibrated with the calcitic sediment (–2.0 to –4.0 ‰). The observed $\Delta^{18}O_{bio\text{-}bulk}$ can be explained through an addition of authigenic carbonate ($F_{CaCO_3(au)}$ = 0.2-0.3; Fig. 8). This model implies diagenetic stabilization at low water/rock ratios (< 10), which is typical for carbonates that stabilize in contact only with marine/pore water-sourced fluid, in the marine phreatic environment under “closed system” diagenesis.

The vertical shifts in the bulk-rock $\delta^{18}O$ profiles of the two study sections match those of the brachiopod/conodont $\delta^{18}O$ profiles (Joachimski et al., 2012; Schobben et al., 2014). This is an additional strong argument that lithification and diagenetic stabilization of the whole-rock carbonate occurred in a closed system, resulting in a relatively uniform offset of the $\delta^{18}O$ values of secondary carbonate phases relative to those of well-preserved biogenic carbonates. The study sections, thus, exhibit partial retention of their primary marine carbon and oxygen isotope signals, preserving the

original pattern of stratigraphic variations in $\delta^{13}C$ and $\delta^{18}O$ despite negative offsets of up to several per mille due to diagenetic influences.

6. Discussion

6.1. Permian-Triassic carbonate $\delta^{13}C$-$\delta^{18}O$ records

Uppermost Permian-Lower Triassic sections globally are characterized by large positive and negative excursions in carbonate $\delta^{13}C$. The interval bracketing the Permian-Triassic (P-Tr) boundary (251.902 ± 0.024 Ma; Burgess et al., 2014) is associated with a large negative $\delta^{13}C$ excursion that has been attributed to a global carbon cycle perturbation (for a review, see Korte and Kozur, 2010). A long-term (~0.5-1.0 Myr) negative carbonate carbon isotope trend started in the latest Permian and continued into the earliest Triassic, a feature characteristic of many P-Tr successions around the globe (e.g., Baud et al 1989; Hermann et al., 2010; Korte and Kozur, 2010; Korte et al., 2010; Tong et al., 2007; Fig. 6). This "first-order $\delta^{13}C$ trend" has been attributed to the effects of Siberian Traps volcanism (Sobolev et al., 2011) including the metamorphism of organic-rich sediments (Korte et al., 2010; Retallack and Krull, 2006; Svensen et al., 2009), as well as to the erosion of continental organic matter (Holser and Magaritz, 1987; Kraus et al., 2013; see also Sephton et al., 2005), and the reduction of marine primary productivity (Rampino and Caldeira, 2005). Superimposed fluctuations around the long-term carbon isotope trend have been reported (e.g., Algeo et al., 2007, 2008), and in the present study these short-term fluctuations are referred to as "second-order excursions" (Fig. 6). The latter have been employed to recognize short stratigraphic intervals including individual lithological horizons (e.g., Richoz et al., 2010). For example, a short-term (~2-20 kyr) negative $\delta^{13}C$ excursion coincident with the EPME horizon at Meishan (South China; Fig. 6) (Cao et al., 2009; Burgess et al., 2014) has been attributed to

massive CH_4 release from methane clathrate dissociation (Benton and Twitchett, 2003; Berner, 2002) or rapid expansion of methanogenic species (Rothman et al., 2014).

A bulk-carbonate oxygen isotope record from material of the Gartnerkofel core (Southern Alps) has been interpreted to reflect a temperature rise of 5 °C across the P-Tr boundary (Holser et al., 1989). An even more dramatic temperature rise (~10 °C) has been established based on bulk-carbonate $\delta^{18}O$ from another outcrop in the Southern Alps (Kearsey et al., 2009). However, both these sites are marked by pervasive dolomitization, and the original whole-rock $\delta^{18}O$ values have likely been altered. In addition, stabilization of carbonate constituents might be stratigraphically and spatially heterogeneous, tracking diagenetic and dolomitization processes (Brand et al., 2012b). The oxygen isotope composition of phosphate locked in conodont apatite is considered to be more resistant to diagenesis because of the highly impermeable nature of this biomineral (Joachimski et al., 2009; Pucéat et al., 2004; Wenzel et al., 2000). A negative $\delta^{18}O$ excursion in conodont apatite slightly above the EPME horizon in South China and NW Iran has been attributed to a seawater temperature increase of 7-10 °C (Joachimski et al., 2012; Schobben et al., 2014; Fig. 3).

6.2. Sea level and the preservation potential of primary bulk-rock isotope compositions

Our comparative analysis of bulk-rock and fossil isotope records combined with quantitative modelling (see Sections 5.2-5.3) leads us to conclude that the first-order trends in the bulk-rock C- and O-isotope profiles represent an environmental/climatic signal. We infer that a major perturbation to the global carbon cycle recorded by the first-order negative $\delta^{13}C$ trend across the EPME coincided with global climatic and tropical seawater temperature warming, as recorded by a parallel shift in $\delta^{18}O$ profiles (cf. Holser et al., 1989). These primary signals can still be recognized despite alteration of absolute C- and O-isotope values through subsequent diagenesis. Diagenesis resulted in negative offsets from primary marine carbonate values in the whole-rock $\delta^{13}C$ and $\delta^{18}O$ records as a result of the influences of elevated burial temperatures and (an)aerobic OC oxidation.

The degree of diagenetic alteration of the C- and O-isotope records appears to have been fairly uniform throughout the study sections, possibly owing to limited lithologic variation and generally similar burial conditions at the time of diagenesis. Conodont CAI values and modelling constraints (see Section 5.3) suggest that diagenetic stabilization of carbonate occurred at relatively low burial temperatures and, hence, shallow depths within the marine phreatic zone.

The study units show no evidence of alteration by meteoric waters. Platform carbonates that recrystallize when exposed to meteoric (carbonate-undersaturated) waters show features of strong dissolution, high water-rock ratios ("open system"), and low $\delta^{18}O$ compositions owing to the ^{18}O-depleted nature of the meteoric fluid. The $\delta^{13}C$ compositions of secondary carbonates forming in open diagenetic systems are typically variable but more depleted than the primary marine carbonate owing to incorporation of ^{13}C-depleted carbon from oxidation of OC (Brand and Veizer, 1981; Knauth and Kennedy, 2009; Marshall, 1992). The lack of evidence of meteoric influence in the study units suggests that sea-level elevations remained high during their deposition. This inference is consistent with the hypothesis of a global marine transgression during the latest Permian-Early Triassic (for a review, see Hallam and Wignall, 1999). Although it has been proposed that the boundary beds, especially on Chinese carbonate platforms, are marked by an erosional surface (Yin et al., 2014) and show signs of subaerial exposure (Collin et al., 2009), the sedimentological evidence is controversial and the supposed karstic surfaces have also been suggested to originate from a submarine dissolution event (Payne et al., 2007). Furthermore, the present study sections as well as other PTB carbonate successions globally (Fig. 4B) are marked by generally heavy carbon isotope compositions despite variable and commonly light $\delta^{18}O$ values. This pattern is consistent with marine phreatic diagenesis under high sea-level conditions, a scenario that offers strong potential for preserving the original marine chemistry of both the bulk-carbonate sediment and biogenic calcite components.

6.3. Significance of authigenic carbonate precipitation

Precipitation of ^{13}C-depleted secondary carbonate phases at a large scale can potentially influence the global carbon cycle. Although carbonate dissolution related to CO_2 production typically accompanies aerobic decay of organic matter in the shallow diagenetic environment (see Section 5.2), subsequent decay reactions in the anoxic deeper sediment column lead to increased pore water alkalinity and precipitation of authigenic carbonate phases. These processes include microbial sulfate reduction (MSR) (Emerson and Hedges, 2003; Shen and Buick, 2004) and anaerobic oxidation of methane (AOM) (Boetius et al., 2000; Hinrichs et al., 1999). Detection and quantification of authigenic carbonate precipitation through Earth history might be of quantitative importance for global carbon budgets, as suggested by Schrag et al. (2013).

Several considerations suggest that precipitation of authigenic carbonate during the PTB crisis was considerable and possibly influenced the contemporaneous global carbon cycle. The fraction of authigenic carbonate in the study samples is calculated at 20-30 % of the total rock weight (Section 5.3), a value which lies at the upper range observed for modern carbonate deposits (Schrag et al., 2013 and references therein). Sufficiently large-scale precipitation of isotopically light authigenic carbonate in essence sequesters ^{13}C-depleted organic carbon (in oxidized form) in the sediment, preventing it from diffusing back into the overlying water column and, thus, contributing to an increase in the $\delta^{13}C$ of global dissolved inorganic carbon (DIC). A related consideration is that widespread oceanic dysoxia/anoxia, as during the latest Permian-Early Triassic (Wignall and Twitchett, 1996; Brennecka et al., 2011), decreases the total amount of aerobic oxidation of OC in sediments globally and increases the amount of anaerobic oxidation, leading to a general increase in pore water alkalinity and widespread precipitation of authigenic carbonates (Schrag et al. 2013). This process should be accompanied by heavy $\delta^{13}C$ of seawater DIC owing to increased sequestration of isotopically light carbon in authigenic carbonate phases. This diagenetic C sink provides an alternative explanation for the enriched $\delta^{13}C$ in bulk carbonate sediments and calcite biogens of the Late Permian (before the onset of the secular negative trend towards lighter

$\delta^{13}C$ values). These carbonates with enriched $\delta^{13}C$ are some of the heaviest values recorded for the Phanerozoic (Veizer et al., 1999), a feature which has formerly been interpreted as the result of elevated OC burial (e.g., Rothman et al., 2014). Incorporation of this diagenetic feature into our current understanding of Permian-Triassic seawater chemistry evolution suggests the need for a wide-ranging re-evaluation of bulk-rock carbonate isotope data.

6.4. Second-order carbon isotope excursions: globally correlative signals or local diagenetic effects?

Second-order isotope excursions represent short-term deviations from the general first-order trend towards lower $\delta^{13}C$ and $\delta^{18}O$ up-section, as shown in our case study of P-Tr boundary beds. In the present study, second-order isotope excursions are confined to narrow stratigraphic intervals, covered by only a few data points, and often associated with a certain lithology (Fig. 6). These stratigraphically restricted isotope fluctuations contrast with the first-order isotope trends, which cut across several different lithologies and, thus, are clearly not controlled by lithology.

Many PTB sections exhibit small-scale second-order fluctuations in bulk-carbonate $\delta^{13}C$ superimposed on the general negative trend (Cao et al., 2009; Korte et al., 2004a). At multiple PTB sections, Heydari et al. (2001) attributed these features to meteoric diagenesis related to a subaerial exposure surface, although $\delta^{13}C$-$\delta^{18}O$ covariation patterns do not support this interpretation (cf. Fig. 4) and the evidence for subaerial exposure is weak (n.b., observed features in this section are more likely due to submarine dissolution; Leda et al., 2014). At Nhi Tao, Vietnam, Algeo et al. (2008) demonstrated that second-order $\delta^{13}C$ fluctuations were closely associated with framboidal pyrite layers having strongly negative $\delta^{34}S_{py}$ values and, on this basis, inferred an origin through upward chemocline excursions (cf. Kump et al., 2005).

In the present study sections, second-order $\delta^{13}C$ fluctuations, which are especially evident in the Boundary Clay, are likely to have been the product of late-stage diagenesis. This inference is

based on the relationship of these features to variations in lithology and Mg/Ca ratios (Fig. 6). A similar pattern is seen in the Meishan D section, in which high Mg/Ca is associated with second-order positive $\delta^{13}C$ excursions within the clay-rich boundary interval (Fig. 6), and was attributed to late-stage dolomitization by Xie and Wang (2011). These considerations suggest that second-order $\delta^{13}C$ excursions frequently (although not always) have a diagenetic origin that precludes their use as stratigraphic markers (e.g., Xie et al., 2007; Hermann et al., 2011).

Distinguishing an environmental from a diagenetic origin for second-order bulk-rock $\delta^{13}C$ and $\delta^{18}O$ excursions remains difficult. Patterns of covariation between carbonate C- and O-isotopes and elemental data are not diagnostic of diagenesis, because environmental and biological influences on calcite precipitation can mimic known diagenetic patterns (see Section 6.1). Furthermore, if diagenetic artefacts are restricted to narrow stratigraphic intervals or specific lithologies (as in the present study units), then the isotopic-elemental relationships indicative of such an origin can be obscured when data for larger stratigraphic intervals are lumped together. A robust approach to assessing the influence of local diagenesis on bulk-carbonate C- and O-isotopes would entail fossil versus bulk-rock comparisons combined with elemental and TOC data at a sufficiently high stratigraphic resolution to allow recognition of the diagenetic signals, as demonstrated in the present study.

7. Conclusions

Fossils of brachiopods and conodonts that are well-preserved and minimally altered diagenetically are favoured as proxies for primary marine isotopic compositions, although their abundance and spatial distribution in many successions can be insufficient for construction of a continuous isotopic profile. For this reason, the C- and, less often, O-isotopic compositions of bulk-carbonate have been used in palaeoenvironmental studies, commonly with assessment of diagenetic alteration through examination of elemental ratios (e.g., Mn/Ca, Sr/Ca). However, the application of

elemental screening to identify the extent of diagenetic alteration of calcite samples can lead to uncertain results owing to environmental controls on these proxies. In this study, we have shown that continuous isotopic profiles based on bulk-rock analyses can be tested for diagenetic influences and preservation of a primary marine trend by comparison with limited C- and O-isotope data from biogenic components. For carbonate successions, limited diagenetic alteration is most likely to be encountered when post-depositional stabilization occurs in a marine phreatic environment, i.e., without exposure to meteoric fluids as a result of sea-level fall.

With regard to the present study sections, the first-order negative $\delta^{13}C$ excursion across the P-Tr boundary at Kuh-e-Ali Bashi and Zal (as well as many sections globally) is a secular feature that was caused by a major carbon cycle perturbation. However, small-scale secondary fluctuations in $\delta^{13}C$, especially in the Boundary Clay, appear related to lithologic variation. This observation suggests that such small-scale isotopic features should be interpreted with caution and only used for palaeoenvironmental interpretation if they can be independently verified in multiple coeval successions. The presence of substantial amounts of isotopically light carbon in the study sections may be due to enhanced precipitation of authigenic carbonate, as evidenced by modelling of the observed offsets in the C and O isotope signatures of different compenents in the carbonate rock. This observation has implications for the global carbon cycle, suggesting that authigenic carbonates may play an important role as a carbon sink.

Acknowledgments

We acknowledge the Aras Free Zone office and particularly Adel Najafzadeh (Tabriz) for permission to sample the Kuh-e-Ali Bashi and Zal sites. We sincerely thank Kathrin Krahn, Melanie Rühl and Carina Klein (Museum für Naturkunde Berlin) for technical assistance. We are grateful for assistance with statistical analysis by Melanie Tietje and editorial work by Sonny A. Walton (Museum für Naturkunde). TJA thanks the Sedimentary Geology and Paleobiology program of the U.S. National Science Foundation, the NASA Exobiology program, and the China University

of Geosciences-Wuhan (SKL-GPMR program GPMR201301, and SKL-BGEG program BGL21407) for support. This study was funded by Deutsche Forschungsgemeinschaft (DFG; projects KO1829/12-1, KO1829/12-2 and KO2011/8-1).

References

Al-Aasm, I.S., Veizer, J., 1986. Diagenetic stabilization of aragonite and low-Mg calcite; I, Trace elements in rudists. Journal of Sedimentary Petrology 56, 138-152.

Algeo, T.J., 1996. Meteoric water/rock ratios and the significance of sequence and parasequence boundaries in the Gobbler Formation (Middle Pennsylvanian) of south-central New Mexico. In: Witzke, B.J., Ludvigson, G.A., Day, J. (eds.), Paleozoic Sequence Stratigraphy: Views from the North American Craton, Geological Society of America Special Paper 306, pp. 359-371.

Algeo, T.J., Wilkinson, B.H., Lohmann, K.C., 1992. Meteoric burial diagenesis of Middle Pennsylvanian limestones in the Orogrande Basin, New Mexico: Water/Rock interactions and basin geothermics. Journal of Sedimentary Petrology 62, 652-670.

Algeo, T.J., Ellwood, B.B., Nguyen, T.K.T., Rowe, H., Maynard, J.B., 2007. The Permian-Triassic boundary at Nhi Tao, Vietnam: Evidence for recurrent influx of sulfidic watermasses to a shallow-marine carbonate platform. Palaeogeography Palaeoclimatology Palaeoecology 252, 304-327.

Algeo, T.J., Shen, Y., Zhang, T., Lyons, T.W., Bates, S.M., Rowe, H., Nguyen, T.K.T., 2008. Association of ^{34}S-depleted pyrite layers with negative carbonate δ^{13}C excursions at the Permian/Triassic boundary: Evidence for upwelling of sulfidic deep-ocean watermasses. Geochemistry Geophysics Geosystems 9, Q04025, 10 pp.

Algeo, T.J., Henderson, C.M., Tong, J., Feng, Q., Yin, H., Tyson, R.V., 2013. Plankton and productivity during the Permian–Triassic boundary crisis: An analysis of organic carbon fluxes. Global and Planetary Change 105, 52-67.

Auguie, B., 2012. gridExtra: functions in Grid graphics, R package version 0.9.1. ed.

Banner, J.L., 1995. Application of the trace element and isotope geochemistry of strontium to studies of carbonate diagenesis. Sedimentology 42, 805-824.

Banner, J.L., Hanson, G.N., 1990. Calculation of simultaneous isotopic and trace element variations during water-rock interaction with applications to carbonate diagenesis. Geochimica et Cosmochimica Acta 54, 3123-3137.

Bathurst, R.G.C., 1976. Carbonate Sediments and Their Diagenesis, 2nd ed. Elsevier, Amsterdam, 660 pp.

Baud, A., Magaritz, M., Holser, W., 1989. Permian-Triassic of the Tethys: Carbon isotope studies. Geologische Rundschau 78, 649-677.

Benton, M.J., Twitchett, R.J., 2003. How to kill (almost) all life: the end-Permian extinction event. Trends in Ecology and Evolution 18, 358-365.

Berner, R. A., 2002. Examination of hypotheses for the Permo-Triassic boundary extinction by carbon cycle modeling. Proceedings of the National Academy of Sciences (U.S.A.) 99, 4172-4177.

Boetius, A., Ravenschlag, K., Schubert, C.J., Rickert, D., Widdel, F., Gieseke, A., Amann, R., Jorgensen, B.B., Witte, U., Pfannkuche, O., 2000. A marine microbial consortium apparently mediating anaerobic oxidation of methane. Nature 407, 623-626.

Brand, U., 1989. Global climatic changes during the Devonian-Mississippian: Stable isotope biogeochemistry of brachiopods. Global and Planetary Change 1, 311-329.

Brand, U., Veizer, J., 1980. Chemical diagenesis of a multicomponent carbonate system - 1: Trace elements. Journal of Sedimentary Petrology 50, 1219-1236.

Brand, U., Veizer, J., 1981. Chemical diagenesis of a multicomponent carbonate system - 2: stable isotopes. Journal of Sedimentary Petrology 51, 987-997.

Brand, U., Logan, A., Hiller, N., Richardson, J., 2003. Geochemistry of modern brachiopods: applications and implications for oceanography and paleoceanography. Chemical Geology 198, 305-334.

Brand, U., Jiang, G., Azmy, K., Bishop, J., Montanez, I.P., 2012a. Diagenetic evaluation of a Pennsylvanian carbonate succession (Bird Spring Formation, Arrow Canyon, Nevada, USA)-1: Brachiopod and whole rock comparison. Chemical Geology 308, 26-39.

Brand, U., Posenato, R., Came, R., Affek, H., Angiolini, L., Azmy, K., Farabegoli, E., 2012b. The end-Permian mass extinction: A rapid volcanic CO_2 and CH_4-climatic catastrophe. Chemical Geology 322, 121-144.

Brennecka, G.A., Herrmann, A.D., Algeo, T.J., Anbar, A.D., 2011. Rapid expansion of oceanic anoxia immediately before the end-Permian mass extinction. Proceedings of the National Academy of Sciences (U.S.A.) 108(43), 17631-17634.

Buggisch, W., Joachimski, M.M., 2006. Carbon isotope stratigraphy of the Devonian of Central and Southern Europe. Palaeogeography, Palaeoclimatology, Palaeoecology 240, 68-88.

Burgess, S.D., Bowring, S., Shen, S.Z., 2014. High-precision timeline for Earth's most severe extinction. Proceedings of the National Academy of Sciences (U.S.A.) 111, 3316-3321.

Cao, C., Love, G.D., Hays, L.E., Wang, W., Shen, S., Summons, R.E., 2009. Biogeochemical evidence for euxinic oceans and ecological disturbance presaging the end-Permian mass extinction event. Earth and Planetary Science Letters 281, 188-201.

Collin, P.-Y., Kershaw, S., Crasquin-Soleau, S., Feng, Q., 2009. Facies changes and diagenetic processes across the Permian-Triassic boundary event horizon, Great Bank of Guizhou, South China: a controversy of erosion and dissolution. Sedimentology 56, 677-693.

Denison, R.E., Koepnick, R.B., Fletcher, A., Howell, M.W., Callaway, W.S., 1994. Criteria for the retention of original seawater $^{87}Sr^{86}Sr$ in ancient shelf limestones. Chemical Geology 112, 131-143.

Emerson, S., Hedges, J., 2003. Sediment diagenesis and benthic flux. In: Holland, H.D., Turekian, K.K. (eds.), Treatise on Geochemistry: The Oceans and Marine Geochemistry. Elsevier, Amsterdam, pp. 293-319.

Emrich, K., Ehhalt, D.H., Vogel, J.C., 1970. Carbon isotope fractionation during the precipitation of calcium carbonate. Earth and Planetary Science Letters 8, 363-371.

Flügel, E., 2004. Microfacies of Carbonate Rocks. Springer, Berlin, Germany, 976 pp.

Ghaderi, A., Leda, L., Schobben, M., Korn, D., Ashouri, A.R., 2014. High-resolution stratigraphy of the Changhsingian (Late Permian) successions of NW Iran and the Transcaucasus based on lithological features, conodonts and ammonoids. Fossil Record 17, 41-57.

Haas, J., Demény, A., Hips, K., Vennemann, T.W., 2006. Carbon isotope excursions and microfacies changes in marine Permian–Triassic boundary sections in Hungary. Palaeogeography, Palaeoclimatology, Palaeoecology 237, 160-181.

Hallam, A., Wignall, P.B., 1999. Mass extinctions and sea-level changes. Earth-Science Reviews 48, 217-250.

Hermann, E., Hochuli, P.A., Bucher, H., Vigran, J.O., Weissert, H., Bernasconi, S.M., 2010. A close-up view of the Permian–Triassic boundary based on expanded organic carbon isotope records from Norway (Trøndelag and Finnmark Platform). Global and Planetary Change 74, 156-167.

Hermoso, M., Minoletti, F., Rickaby, R.E.M., Hesselbo, S.P., Baudin, F., Jenkyns, H.C., 2012. Dynamics of a stepped carbon-isotope excursion: Ultra high-resolution study of Early Toarcian environmental change. Earth and Planetary Science Letters 319-320, 45-54.

Heydari, E., Wade, W.J., Hassanzadeh, J., 2001. Diagenetic origin of carbon and oxygen isotope compositions of Permian-Triassic boundary strata. Sedimentary Geology 143, 191-197.

Heydari, E., Hassanzadeh, J., Wade, W.J., Ghazi, A.M., 2003. Permian-Triassic boundary interval in the Abadeh section of Iran with implications for mass extinction: Part 1-Sedimentology. Palaeogeography Palaeoclimatology Palaeoecology 193, 405-423.

Hinrichs, K.U., Hayes, J.M., Sylva, S.P., Brewer, P.G., DeLong, E.F., 1999. Methane-consuming archaebacteria in marine sediments. Nature 398, 802-805.

Holser, W.T., Magaritz, M., 1987. Events near the Permian–Triassic boundary. Modern Geology 11, 155–180.

Holser, W.T., Schönlaub, H.-P., Attrep, M., Boeckelmann, K., Klein, P., Magaritz, M., Orth, C.J., Fenninger, A., Jenny, C., Kralik, M., 1989. A unique geochemical record at the Permian/Triassic boundary. Nature 337, 39-44.

Horacek, M., Richoz, S., Brandner, R., Krystyn, L., Spötl, C., 2007. Evidence for recurrent changes in Lower Triassic oceanic circulation of the Tethys: The $\delta^{13}C$ record from marine sections in Iran. Palaeogeography, Palaeoclimatology, Palaeoecology 252, 355-369.

Imai, N., Terashima, S., Itoh, S., Ando, A., 1996. Compilation of analytical data on nine GSJ geochemical reference samples, "Sedimentary rock series". Geostandards Newsletter 20, 165-216.

Jenkyns, H.C., Clayton, C.J., 1986. Lower Jurassic epicontinental carbonates and mudstones from England and Wales: chemostratigraphic signals and the early Toarcian anoxic event. Sedimentology 44, 687-706.

Jin, Y.G., Wang, Y., Wang, W., Shang, Q.H., Cao, C.Q., Erwin, D.H., 2000. Pattern of marine mass extinction near the Permian-Triassic boundary in South China. Science 289, 432-436.

Joachimski, M.M., Breisig, S., Buggisch, W., Talent, J.A., Mawson, R., Gereke, M., Morrow, J.R., Day, J., Weddige, K., 2009. Devonian climate and reef evolution: Insights from oxygen isotopes in apatite. Earth and Planetary Science Letters 284, 599-609.

Joachimski, M.M., Lai, X., Shen, S., Jiang, H., Luo, G., Chen, B., Chen, J., Sun, Y., 2012. Climate warming in the latest Permian and the Permian-Triassic mass extinction. Geology 40, 195-198.

Kaufman, A.J., Knoll, A.H., 1995. Neoproterozoic variations in the C-isotopic composition of seawater: stratigraphic and biogeochemical implications. Precambrian Research 73, 27-49.

Kearsey, T., Twitchett, R.J., Price, G.D., Grimes, S.T., 2009. Isotope excursions and palaeotemperature estimates from the Permian/Triassic boundary in the Southern Alps (Italy). Palaeogeography, Palaeoclimatology, Palaeoecology 279, 29-40.

Kim, S.T., O'Neil, J.R., 1997. Equilibrium and nonequilibrium oxygen isotope effects in synthetic carbonates. Geochimica et Cosmochimica Acta 61, 3461-3475.

Knauth, L.P., Kennedy, M.J., 2009. The late Precambrian greening of the Earth. Nature 460, 728-732.

Knoll, A.H., Hayes, J.M., Kaufman, A.J., Swett, K., Lambert, I.B., 1986. Secular variation in carbon isotope ratios from Upper Proterozoic successions of Svalbard and East Greenland. Nature 321, 832-838.

Knoll, A.H., Bambach, R.K., Payne, J.L., Pruss, S., Fischer, W.W., 2007. Paleophysiology and end-Permian mass extinction. Earth and Planetary Science Letters 256, 295-313.

Korte, C., Hesselbo, S.P., 2011. Shallow marine carbon and oxygen isotope and elemental records indicate icehouse–greenhouse cycles during the Early Jurassic. Paleoceanography 26, PA4219, doi:10.1029/2011PA002160.

Korte, C., Kozur, H.W., 2005. Carbon isotope stratigraphy across the Permian/Triassic boundary at Jolfa (NW-Iran), Peitlerkofel (Sass de Pütia, Sass de Putia), Pufels (Bula, Bulla), Tesero (all three Southern Alps, Italy) and Gerennavár (Bükk Mts., Hungary). Journal of Alpine Geology 47, 119-135.

Korte, C., Kozur, H.W., 2010. Carbon isotope stratigraphy across the Permian–Triassic boundary: a review. Journal of Asian Earth Sciences 39, 215–235.

Korte, C., Kozur, H.W., Bruckschen, P., Veizer, J., 2003. Strontium isotope evolution of Late Permian and Triassic seawater. Geochimica et Cosmochimica Acta 67, 47–62.

Korte, C., Kozur, H.W., Joachimski, M.M., Strauss, H., Veizer, J., Schwark, L., 2004a. Carbon, sulfur, oxygen and strontium isotope records, organic geochemistry and biostratigraphy across the Permian/Triassic boundary in Abadeh, Iran. International Journal of Earth Sciences 93, 565–581.

Korte, C., Kozur, H.W., Mohtat-Aghai, P., 2004b. Dzhulfian to lowermost Triassic $\delta^{13}C$ record at the Permian/Triassic boundary section at Shahreza, Central Iran. Hallesches Jahrbuch für Geowissenschaften B18, 73–78.

Korte, C., Kozur, H.W., Partoazar, H., 2004c. Negative carbon isotope excursion at the Permian/Triassic boundary section at Zal, NW Iran. Hallesches Jahrbuch für Geowissenschaften B18, 69-71.

Korte, C., Jasper, T., Kozur, H.W., Veizer, J., 2005a. $\delta^{18}O$ and $\delta^{13}C$ of Permian brachiopods: A record of seawater evolution and continental glaciation. Palaeogeography, Palaeoclimatology, Palaeoecology 224, 333-351.

Korte, C., Kozur, H.W., Veizer, J., 2005b. $\delta^{13}C$ and $\delta^{18}O$ values of Triassic brachiopods and carbonate rocks as proxies for coeval seawater and palaeotemperature. Palaeogeography, Palaeoclimatology, Palaeoecology 226, 287-306.

Korte, C., Pande, P., Kalia, P., Kozur, H.W., Joachimski, M.M., Oberhänsli, H., 2010. Massive volcanism at the Permian–Triassic boundary and its impact on the isotopic composition of the ocean and atmosphere. Journal of Asian Earth Sciences 37, 293–311.

Kozur, H.W., 2007. Biostratigraphy and event stratigraphy in Iran around the Permian-Triassic Boundary (PTB): Implications for the causes of the PTB biotic crisis. Global and Planetary Change 55, 155-176.

Kraus, S.H., Siegert, S., Mette, W., Struck, U., Korte, C., 2009. Stratigraphic significance of carbon isotope variations in the shallow-marine Seis/Siusi Permian–Triassic boundary section (Southern Alps, Italy). Fossil Record 12 (2), 197-205.

Kraus, S.H., Brandner, R., Heubeck, C., Kozur, H.W., Struck, U., Korte, C., 2013. Carbon isotope signatures of latest Permian marine successions of the Southern Alps suggest a continental runoff pulse enriched in land plant material. Fossil Record 16 (1), 97-109.

Kump, L.R., Pavlov, A., Arthur, M.A., 2005. Massive release of hydrogen sulfide to the surface ocean and atmosphere during intervals of oceanic anoxia. Geology 33, 397-400.

Leda, L., Korn, D., Ghaderi, A., Hairapetian, V., Struck, U., Reimold, W.U., 2014. Lithostratigraphy and carbonate microfacies across the Permian–Triassic boundary near Julfa (NW Iran) and in the Baghuk Mountains (Central Iran). Facies 59, 1-31.

Luo, G., Kump, L.R., Wang, Y., Tong, J., Arthur, M.A., Yang, H., Huang, J., Yin, H., Xie, S., 2010. Isotopic evidence for an anomalously low oceanic sulfate concentration following end-Permian mass extinction. Earth and Planetary Science Letters 300, 101-111.

Marshall, J.D., 1992. Climatic and oceanographic isotopic signals from the carbonate rock record and their preservation. Geological Magazine 129, 143-160.

Marshall, J.D., Middleton, P.D., 1990. Changes in marine isotopic composition and the late Ordovician glaciation. Journal of the Geological Society of London 147, 1-4.

McHargue, T.R., Price, R.C., 1982. Dolomite from clay in argillaceous or shale-associated marine carbonates. Journal of Sedimentary Petrology 52, 873-886.

Melim, L.A., Westphal, H., Swart, P.K., Eberli, G.P., Munnecke, A., 2002. Questioning carbonate diagenetic paradigms: evidence from the Neogene of the Bahamas. Marine Geology 185, 27-53.

Middelburg, J.J., De Lange, G.J., van Der Weijden, C.H., 1987. Manganese solubility control in marine pore waters. Geochimica et Cosmochimica Acta 51, 759-763.

Mii, H.-S., Grossman, E.L., Yancey, T.E., 1999. Carboniferous isotope stratigraphies of North America: Implications for Carboniferous paleoceanography and Mississippian glaciation. Geological Society of America Bulletin 111, 960-973.

Mohtat Aghai, P., Vachard, D., Krainer, K., 2011. Transported foraminifera in Palaeozoic deep red nodular limestones exemplified by latest Permian Neoendothyra in the Zal section (Julfa area, NW Iran). Revista Española de Micropaleontología 41, 197-213.

Munnecke, A., Westphal, H., Reijmer, J.J.G., Samtleben, C., 1997. Microspar development during early marine burial diagenesis: a comparison of Pliocene carbonates from the Bahamas with Silurian limestones from Gotland (Sweden). Sedimentology 44, 977-990.

Payne, J.L., Lehrmann, D.J., Wei, J.Y., Orchard, M.J., Schrag, D.P., Knoll, A.H., 2004. Large perturbations of the carbon cycle during recovery from the end-Permian extinction. Science 305, 506-509.

Payne, J.L., Lehrmann, D.J., Follett, D., Seibel, M., Kump, L.R., Riccardi, A., Altiner, D., Sano, H., Wei, J.Y., 2007. Erosional truncation of uppermost Permian shallow-marine carbonates and implications for Permian-Triassic boundary events. Geological Society of America Bulletin 119, 771-784.

Pingitore, N.E., Jr., 1978. The behavior of Zn^{2+} and Mn^{2+} during carbonate diagenesis; theory and applications. Journal of Sedimentary Petrology 48, 799-814.

Pingitore, N.E., Jr., Eastman, M.P., Sandidge, M., Oden, K., Freiha, B., 1988. The coprecipitation of manganese(II) with calcite: an experimental study. Marine Chemistry 25, 107-120.

Pucéat, E., Reynard, B., Lécuyer, C., 2004. Can crystallinity be used to determine the degree of chemical alteration of biogenic apatites? Chemical Geology 205, 83-97.

Rampino, M.R., Caldeira, K., 2005. Major perturbation of ocean chemistry and a 'Strangelove Ocean' after the end-Permian mass extinction. Terra Nova 17, 554-559.

R Core Team, 2014. A language and environment for statistical computing. R Foundation for Statistical Computing, Vienna, Austria.

Retallack, G.J., Krull, E.S., 2006. Carbon isotopic evidence for terminal-Permian methane outbursts and their role in extinctions of animals, plants, coral reefs, and peat swamps. In: Greb, S.F., DiMichele, W.A. (eds.), Wetlands Through Time, Geological Society of America Special Paper 399, pp. 249-268.

Riccardi, A.L., Arthur, M.A., Kump, L.R., 2006. Sulfur isotopic evidence for chemocline upward excursions during the end-Permian mass extinction. Geochimica et Cosmochimica Acta 70, 5740-5752.

Richoz, S., Krystyn, L., Baud, A., Brandner, R., Horacek, M., Mohtat-Aghai, P., 2010. Permian–Triassic boundary interval in the Middle East (Iran and N. Oman): Progressive environmental change from detailed carbonate carbon isotope marine curve and sedimentary evolution. Journal of Asian Earth Sciences 39, 236-253.

Romano, C., Goudemand, N., Vennemann, T.W., Ware, D., Schneebeli-Hermann, E., Hochuli, P.A., Bruhwiler, T., Brinkmann, W., Bucher, H., 2013. Climatic and biotic upheavals following the end-Permian mass extinction. Nature Geosciences 6, 57-60.

Rothman, D.H., Fournier, G.P., French, K.L., Alm, E.J., Boyle, E.A., Cao, C., Summons, R.E., 2014. Methanogenic burst in the end-Permian carbon cycle. Proceedings of the National Academy of Sciences (U.S.A.) 111, 5462-5467.

Saltzman, M.R., 2002.Carbon isotope ($\delta^{13}C$) stratigraphy across the Silurian–Devonian transition in North America: evidence for a perturbation of the global carbon cycle. Palaeogeography, Palaeoclimatology, Palaeoecology 187, 83-100.

Schlanger, S.O., Arthur, M.A., Jenkyns, H.C., Scholle, P.A., 1987. The Cenomanian-Turonian Oceanic Anoxic Event, I. Stratigraphy and distribution of organic carbon-rich beds and the marine $\delta^{13}C$ excursion. In: Brooks, J., Fleet, A.J. (eds.), Marine Petroleum Source Rocks, Geological Society of London Special Publication 26, pp. 371-399.

Schobben, M., Joachimski, M.M., Korn, D., Leda, L., Korte, C., 2014. Palaeotethys seawater temperature rise and an intensified hydrological cycle following the end-Permian mass extinction. Gondwana Research 26, 675-683.

Schobben, M., Stebbins, A., Ghaderi, A., Strauss, H., Korn, D., Korte, C., 2015. Flourishing ocean drives the end-Permian marine mass extinction. Proceedings of the National Academy of Sciences (U.S.A.) 112, 10298–10303.

Schönlaub, H.P., 1991. The Permian–Triassic of the Gartnerkofel-1 core (Carnic Alps, Austria): conodont biostratigraphy. Abhandlungen der Geologischen Bundesanstalt Wien 45, 79-98.

Schrag, D.P., Higgins, J.A., Macdonald, F.A., Johnston, D.T., 2013. Authigenic carbonate and the history of the global carbon cycle. Science 339, 540-543.

Sephton, M.A., Looy, C.V., Brinkhuis, H., Wignall, P.B., de Leeuw, J.W., Visscher, H., 2005. Catastrophic soil erosion during the end-Permian biotic crisis. Geology 33, 941-944.

Shen, Y., Buick, R., 2004. The antiquity of microbial sulfate reduction. Earth-Science Reviews 64, 243-272.

Siesser, W.G., Rogers, J., 1971. An investigation of the suitability of four methods used in routine carbonate analysis of marine sediments. Deep Sea Research and Oceanographic Abstracts 18, 135-139.

Sobolev, S.V., Sobolev, A.V., Kuzmin, D.V., Krivolutskaya, N.A., Petrunin, A.G., Arndt, N.T., Radko, V.A., Vasiliev, Y.R., 2011. Linking mantle plumes, large igneous provinces and environmental catastrophes. Nature 477, 312-316.

Stampfli, G.M., Borel, G.D., 2002. A plate tectonic model for the Paleozoic and Mesozoic constrained by dynamic plate boundaries and restored synthetic oceanic isochrons. Earth and Planetary Science Letters 196, 17-33.

Stepanov, D.L., Golshani, F., Stocklin, J., 1969. Upper Permian and Permian-Triassic boundary in North Iran. Report of the Geological Survey of Iran 12, 72 pp.

Sternbach, C., Friedman, G., 1986. Dolomites formed under conditions of deep burial: Hunton Group carbonate rocks (Upper Ordovician to Lower Devonian) in the deep Anadarko Basin of Oklahoma and Texas. Carbonates and Evaporites 1, 61-73.

Steuber, T., Veizer, J., 2002. Phanerozoic record of plate tectonic control of seawater chemistry and carbonate sedimentation. Geology 30, 1123-1126.

Sun, Y., Joachimski, M.M., Wignall, P.B., Yan, C., Chen, Y., Jiang, H., Wang, L., Lai, X., 2012. Lethally hot temperatures during the early Triassic greenhouse. Science 338, 366-370.

Svensen, H., Planke, S., Polozov, A.G., Schmidbauer, N., Corfu, F., Podladchikov, Y.Y., Jamtveit, B., 2009. Siberian gas venting and the end-Permian environmental crisis. Earth and Planetary Science Letters 277, 490-500.

Taraz, H., 1971. Uppermost Permian and Permian-Triassic transition beds in central Iran. Bulletin of the American Association of Petroleum Geologists 55, 1280-1294.

Teichert, C., Kummel, B., Sweet, W.C., 1973. Permian-Triassic strata, Kuh-e-Ali Bashi, northwestern Iran. Bulletin of the Museum of Comparative Zoology, Harvard University 145, 359-472.

Tong, J.N., Zuo, J.X., Chen, Z.Q., 2007. Early Triassic isotope excursions from South China: proxies for devastation and restoration of marine ecosystems following the end-Permian mass extinction. Geological Journal 42, 371-389.

Ullmann, C.V., Korte, C., 2015. Diagenetic alteration in low-Mg calcite from macrofossils: A review. Geological Quarterly 59, 3-20.

Ullmann, C.V., Campbell, H.J., Frei, R., Hesselbo, S.P., Pogge von Strandmann, P.A., Korte, C., 2013a. Partial diagenetic overprint of Late Jurassic belemnites from New Zealand: Implications for the preservation potential of δ^7Li values in calcite fossils. Geochimica et Cosmochimica Acta 120, 80-96.

Ullmann, C.V., Hesselbo, S.P., Korte, C., 2013b. Tectonic forcing of Early to Middle Jurassic seawater Sr/Ca. Geology 41, 1211-1214.

Ullmann, C.V., Thibault, N., Ruhl, M., Hesselbo, S. P., Korte, C., 2014. Effect of a Jurassic Oceanic Anoxic Event on belemnite ecology and evolution. Proceedings of the National Academy of Sciences (U.S.A.) 111, 10073-10076.

van Geldern, R., Joachimski, M.M., Day, J., Jansen, U., Alvarez, F., Yolkin, E.A., Ma, X.P., 2006. Carbon, oxygen and strontium isotope records of Devonian brachiopod shell calcite. Palaeogeography, Palaeoclimatology, Palaeoecology 240, 47-67.

Veizer, J., Demovic, R., Turan, J., 1971. Possible use of strontium in sedimentary carbonate rocks as a paleoenvironmental indicator. Sedimentary Geology 5, 5-22.

Veizer, J., Ala, D., Azmy, K., Bruckschen, P., Buhl, D., Bruhn, F., Carden, G.A.F., Diener, A., Ebneth, S., Godderis, Y., Jasper, T., Korte, C., Pawellek, F., Podlaha, O.G., Strauss, H., 1999. ^{87}Sr/^{86}Sr, δ^{13}C and δ^{18}O evolution of Phanerozoic seawater. Chemical Geology 161, 59-88.

Wefer, G., Berger, W.H., 1991. Isotope paleontology: growth and composition of extant calcareous species. Marine Geology 100, 207-248.

Wenzel, B., Lécuyer, C., Joachimski, M.M., 2000. Comparing oxygen isotope records of Silurian calcite and phosphate—$\delta^{18}O$ compositions of brachiopods and conodonts. Geochimica et Cosmochimica Acta 64, 1859-1872.

Wickham, H., 2009. ggplot2: elegant graphics for data analysis. Springer, New York.

Wickham, H., 2012. gtable: Arrange grobs in tables, R package version 0.1.2. ed.

Wignall, P.B., Twitchett, R.J., 1996. Oceanic anoxia and the end Permian mass extinction. Science 272(5265), 1155-1158.

Xie, S., Wang, Y., 2011. Geomicrobiological perspective on the pattern and causes of the 5-million-year Permo/Triassic biotic crisis. Frontiers in Earth Science 5, 23-36.

Xie, S., Pancost, R.D., Huang, J., Wignall, P.B., Yu, J., Tang, X., Chen, L., Huang, X., Lai, X., 2007. Changes in the global carbon cycle occurred as two episodes during the Permian-Triassic crisis. Geology 35, 1083-1086.

Yin, H., Jiang, H., Xia, W., Feng, Q., Zhang, N., Shen, J., 2014. The end-Permian regression in South China and its implication on mass extinction. Earth-Science Reviews 137, 19-33.

Zachos, J. C., Schouten, S., Bohaty, S., Sluijs, A., Brinkhuis, H., Gibbs, S., Bralower, T., Quattlebaum, T., 2006. Extreme warming of mid-latitude coastal ocean during the Paleocene-Eocene Thermal Maximum: Inferences from TEX_{86} and isotope data. Geology 34, 737-740.

Figure and table captions

Fig. 1. (A) Geographical location and (B) palaeogeographic setting of the Kuh-e-Ali Bashi and Zal P-Tr boundary sections in the Julfa region of NW Iran (panel B is adapted from Stampfli and Borel (2002; also Stampfli, pers. comm., 2011). Note that the colouring of the continents in the palaeogeographic map is not indicative of climate zones and biomes.

Fig. 2. (A) Field photo of the Kuh-e-Ali Bashi section. (B-E) Photomicrographs of key lithological and textural features (scale bars = 1 mm). (B) The nodular *Paratirolites* Limestone; note hardground intraclasts ('subsolution clasts') with Fe–Mn crusts and biogenic encrustation on clast rims. Ali Bashi 1, 0.75 m below the EPME horizon. (C) Platy limestone at the base of the *Claraia* Beds showing evidence of recrystallization (e.g., sparry calcite spheres). Ali Bashi 1, 4.15 m above the EPME horizon. (D) The Boundary Clay with abundant rhombic (high-magnesium?) crystals floating in matrix, Ali Bashi 1, 0.40 m above the EPME horizon. (E) The Boundary Clay beds, containing ostracods, sponge remains, and signs of bioturbation. Ali Bashi 1, 0.75 m above the EPME horizon. B and C were adapted from Leda et al. (2014).

Fig. 3. $\delta^{13}C$, $\delta^{18}O$, Mn/Ca, Sr/Ca and Mg/Ca systematics of bulk-carbonate fraction and brachiopod calcite (Schobben et al., 2014) for Kuh-e-Ali Bashi (A) and Zal (B). The conodont $\delta^{18}O$ data taken from Schobben et al. (2014) were converted to the VPDB scale for comparison with carbonate $\delta^{18}O$. The widths of the bars of the conodont $\delta^{18}O$ data represent the different values generated by two different conversion methods (see Section 4.1). Bulk-rock mineralogy, $CaCO_3$, and insoluble residue (IR) are depicted as percentages of total rock. The most salient features of bulk-rock composition are elemental enrichments within the Boundary Clay. In the bulk-rock $\delta^{13}C$ and $\delta^{18}O$ profiles, red circles are used to show samples with elevated Mg/Ca ratios (i.e., values that are >1σ

above the mean). Conodont zones for Kuh-e-Ali Bashi (Kozur, 2007; Ghaderi et al., 2014) and Zal (Schobben et al. 2015) are: (1) *C. changxingensis*, (2) *C. bachmanni*, (3) *C. nodosa*, (4) *C. yini*, (5) *C. abadehensis*, (6) *C. hauschkei*, (7) *H. praeparvus-H. changxingensis*, (8) *M. ultima-S. ?mostleri*, (9) *H. parvus*, (10) *H. lobota*, (11) *I. staeschei*, and (12) *I. isarcica*.

Fig. 4. Cross-plots of (A) Sr/Ca vs Mn/Ca, (B) $\delta^{13}C_{carb}$ vs $\delta^{18}O_{carb}$, (C) Sr/Ca vs $\delta^{13}C_{carb}$, and (D) Mn/Ca vs $\delta^{13}C_{carb}$. Diamonds represent brachiopods and open circles represent bulk-rock samples. In A, data are from Kuh-e-Ali Bashi, Zal (white—this study; Schobben et al., 2014), Val Brutta and Sas de Putia (green—Brand et al., 2012b) and Meishan (blue—Korte et al., 2005a; Riccardi et al., 2006). The Mn/Ca threshold for well-preserved (<0.18 mmol/mol) versus altered (>0.18 mmol/mol) samples is from Denison et al. (1994) and Korte et al. (2003; 2005a). Note that most of the bulk-rock samples fall outside this range. In B, data are from (i) South China and Vietnam (blue), Meishan D (Cao et al., 2009; Korte et al., 2005a), Meishan B (Jin et al., 2000), Nhi Tao (Algeo et al., 2007), and Cili (Luo et al., 2010); (ii) southern Alps and Bükk mountains (green), Val Brutta (Brand et al., 2012b; Kearsey et al., 2009), Sas de Putia (Brand et al., 2012b; Korte and Kozur, 2005), Tesero (Korte and Kozur, 2005), Gartnerkofel (Holser et al., 1989), Bulla (Korte and Kozur, 2005), Gerennavár (Korte and Kozur, 2005), Bálvány (Haas et al., 2006); and (iii) Iran (white), Kuh-e-Ali Bashi, Zal (this study; Korte and Kozur, 2005; Schobben et al., 2014), Abadeh (Korte et al., 2004a). Included is the range of Cenozoic carbon and oxygen isotope values from rocks that lithified under the influence of either marine or meteoric pore water (from Knauth and Kennedy, 2009). The arrows indicate directions of isotopic evolution associated with meteoric and deep burial diagenesis. The pattern observed in the study units is consistent with stabilization in the marine phreatic environment. . In C and D, data are for the Kuh-e-Ali Bashi and Zal sections (this study).

Fig. 5. (A) Mn/Ca and (B) Sr/Ca as a function of lithology (red: Kuh-e-Ali Bashi; blue: Zal). In A, Mn/Ca ratios increase from platy limestone to nodular limestone , and, then, to the Boundary Clay.

In B, Sr/Ca ratios are higher in platy limestone than in nodular limestone, with no consistent pattern for the Boundary Clay. The yellow lines at the bottom represent average values for brachiopod calcite; the ranges of Sr/Ca ratios observed in modern carbonate deposits (Bathurst, 1976) and diagenetic cements (solid—Banner, 1995; dotted—Ullmann and Korte, 2015) are shown on the right side of B.. The black circles are outliers according to the convention of box-and-whisker plots, i.e., values plotting at >1.5× the Interquartile Range (Q_3-Q_1).

Fig. 6. $\delta^{13}C_{carb}$ records for whole-rock samples from Kuh-e-Ali Bashi and Zal (this study—white dots; Korte and Kozur, 2005—grey dots), Abadeh (Korte et al., 2004a), Meishan D (Cao et al., 2009; Korte et al., 2005a), Meishan B (Jin et al., 2000), Gartnerkofel (Holser et al., 1989), and Nhi Tao (Algeo et al., 2007, 2008). Note that the y-axis is scaled with regard to stratigraphic height and relative time; absolute timescale on right for the interval between the EPME horizon and the top of the *H. parvus* zone (based on Burgess et al., 2014). Biostratigraphy and EPME placement are based on: Kuh-e-Ali Bashi and Zal (Ghaderi et al., 2014; Kozur, 2007), Meishan D and B (Jin et al., 2000; Yuan et al., 2014). The stratigraphic subdivision of the Gartnerkofel section is taken from Korte and Kozur (2010) and differs slightly from the original (Schönlaub, 1991). The FAD of *I. staeschei* is not recognized in the sites considered here but is likely analogous to the FAD of *I. isarcica*. A conodont biostratigraphy is not available for Nhi Tao, and correlations are therefore less certain for this section. Red dots represent samples with significant Mg enrichment of the carbonate fraction. The dark grey areas represent carbonate-bearing clay beds or volcanic ash layers, and the light grey areas represent argillaceous limestone and limestone-clay alternations. Dotted vertical lines represent the pre-extinction baseline value for bulk-rock $\delta^{13}C$.

Fig. 7. The offset between biogenic and bulk-rock C-O isotope compositions shown as smoothed trends for Kuh-e-Ali Bashi (A) and Zal (B). The trend lines of bulk-rock $\delta^{13}C$ and $\delta^{18}O$ were generated using a polynomial Kernel regression with a bandwidth equivalent to 1.5× the distance of

the maximum sampling density. The legend for data points is the same as in Figure 3. The histograms show $\Delta^{13}C_{(bio\text{-}bulk)}$, i.e., the difference in C-isotopic compositions of brachiopod and bulk-rock samples. (C) The offset and $\Delta^{18}O_{(bio\text{-}bulk)}$ between conodont and brachiopod (bio) and whole-rock samples (bulk) are for the *Paratirolites* Limestone Member only. (D) The offset and $\Delta^{18}O_{(bio\text{-}bulk)}$ between conodont and brachiopod (bio) and whole-rock samples (bulk) for the complete P-Tr boundary interval. Where the stratigraphic elevations of sample pairs differ, interpolated values were used in Δ calculation.

Fig. 8. Modelling results using parameters for the inferred underlying diagenetic mechanism and offsets between biogenic and bulk rock C-O isotope compositions (Fig. 7). A) Numerical solution for original sedimentary OC based on $\Delta^{13}C_{(bio\text{-}bulk)}$ of 1.2 ‰ (median), based on a range of burial temperatures and $\delta^{13}C$ of the diagenetic fluid. B) Numerical solution for the fraction of authigenic carbonate required to explain an $\Delta^{18}O_{(bio\text{-}bulk)}$ of 2.1 ‰ (median), based on a range of burial temperatures and $\delta^{18}O$ of the diagenetic fluid. C) Graphic representation of whole rock $\delta^{13}C$ under the influence of bicarbonate derived from aerobic OC degradation and the relation to the original sedimentary organic matter content. D) Graphic representation of whole-rock $\delta^{18}O$ as a factor of carbonate originally precipitated from seawater and the diagenetic fluid.

Table 1. Elemental ratios of the international certified standards JLs-1 and JDo-1 (published and measured; element ratios are taken from Imai et al., 1996).

	Sr/Ca (mmol/mol)	**2 sd**	**Mn/Ca (mmol/mol)**	**2 sd**	**Mg/Ca (mmol/mol)**	**2 sd**
JDo-1 (n=3)						
measured	0.21	0.04	0.14	0.02	750.11	21.04
published	0.22		0.15		761.21	
JLs-1 (n=23)						
measured	0.34	0.01	0.03	0.00	14.09	0.24
published	0.34		0.03		15.02	

Table 2. Results for linear model fit between different chemical proxies. The correlation is calculated using Pearson's correlation coefficient (r^2), n = degrees of freedom, p = significance. High Pearson r^2 values indicate a high correlation; low p-values indicate a statistically significant correlation. IR = insoluble residue after acid digestion of a carbonate sample.

	x	**y**				
Section	**(response)**	**(terms)**	**Coefficient**	**Pearson's r^2**	**p-value**	**n**
Kuh-e-Ali Bashi	$\delta^{13}C$	$\delta^{18}O$	0.44	0.73	2.20E-16	78
Zal	$\delta^{13}C$	$\delta^{18}O$	0.51	0.34	5.64E-05	39
Kuh-e-Ali Bashi	Sr/Ca	Mn/Ca	-0.05	0.10	1.00E-02	58
Zal	Sr/Ca	Mn/Ca	-0.04	0.00	7.00E-01	33
Kuh-e-Ali Bashi	Sr/Ca	Mg/Ca	0.00	0.00	6.20E-01	58
Zal	Sr/Ca	Mg/Ca	0.00	0.00	7.80E-01	33
Kuh-e-Ali Bashi	Mn/Ca	$\delta^{13}C$	-0.18	0.02	2.93E-01	57
Zal	Mn/Ca	$\delta^{13}C$	0.27	0.08	9.95E-02	32
Kuh-e-Ali Bashi	Sr/Ca	$\delta^{13}C$	0.71	0.01	5.41E-01	57
Zal	Sr/Ca	$\delta^{13}C$	-0.55	0.11	5.77E-02	32
Kuh-e-Ali Bashi	Mn/Ca	IR	0.05	0.39	2.28E-07	55
Zal	Mn/Ca	IR	0.05	0.34	4.06E-04	31
Kuh-e-Ali Bashi	Sr/Ca	IR	-37.46	0.17	1.43E-03	55
Zal	Sr/Ca	IR	-2.87	0.02	4.59E-01	31

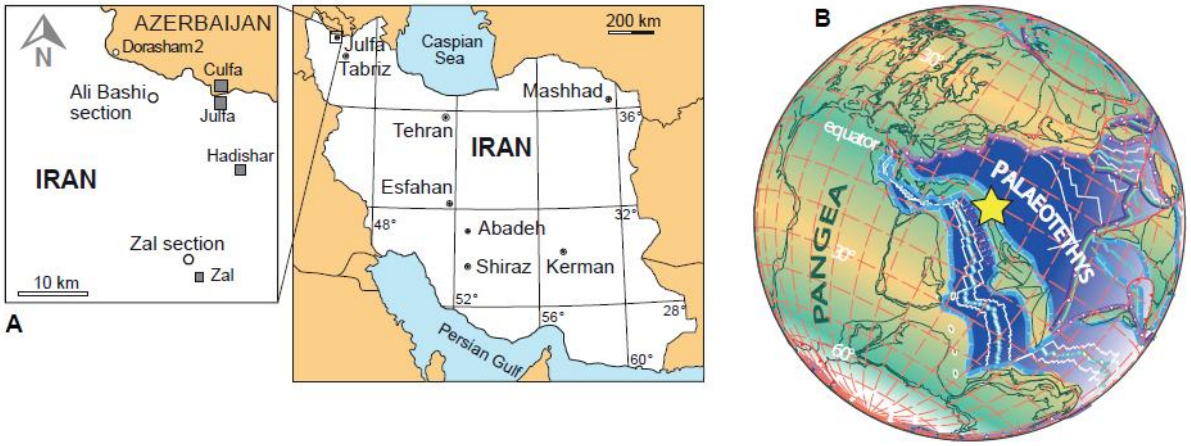

Figure 1

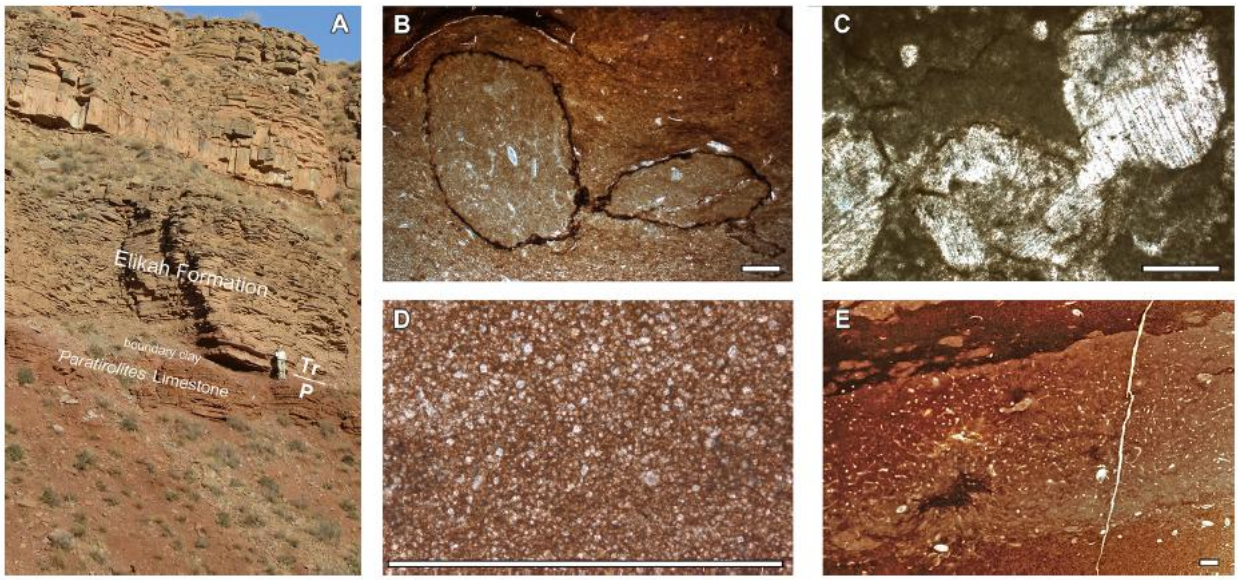

Figure 2

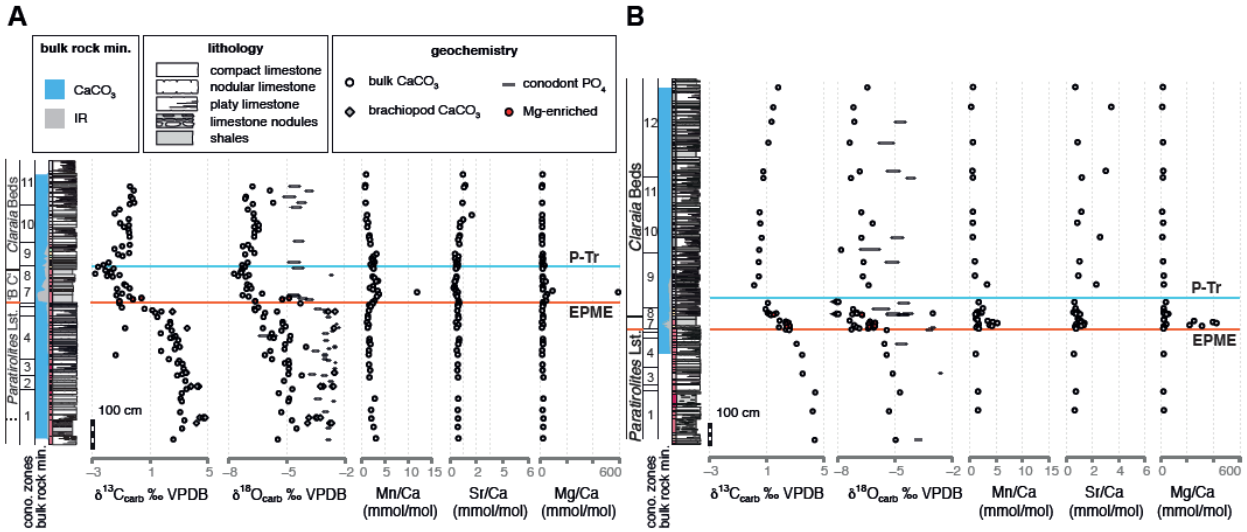

Figure 3

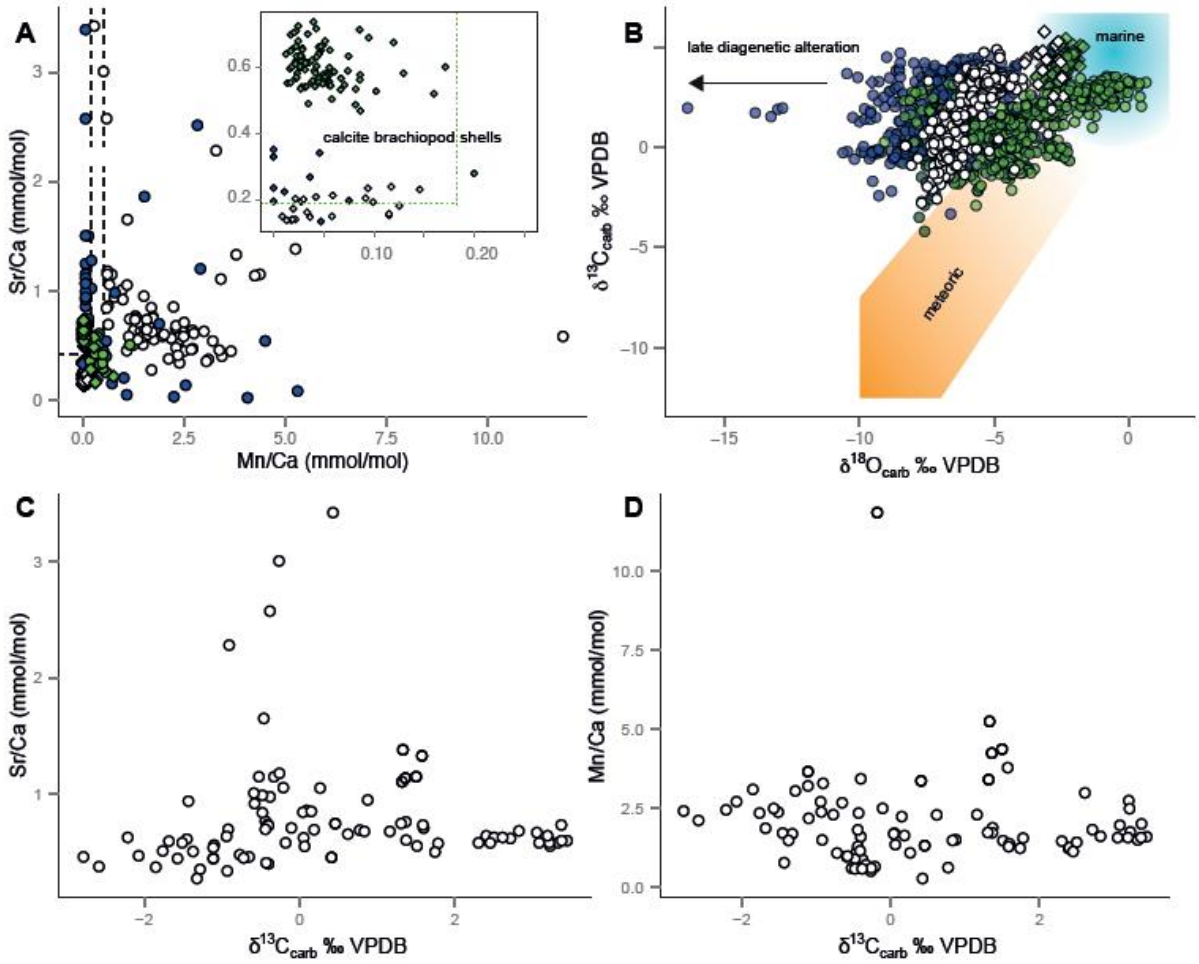

Figure 4

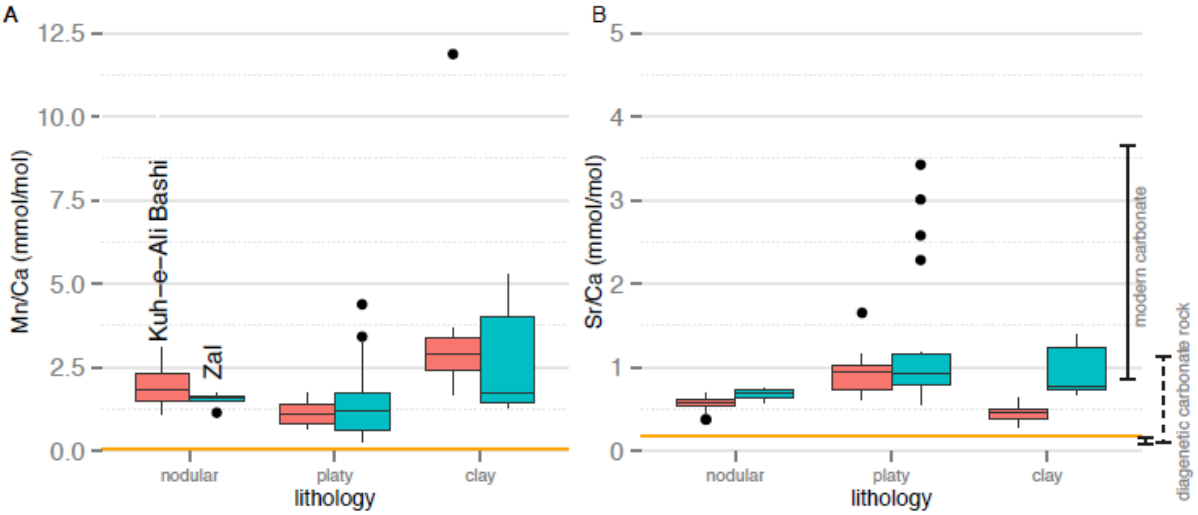

Figure 5

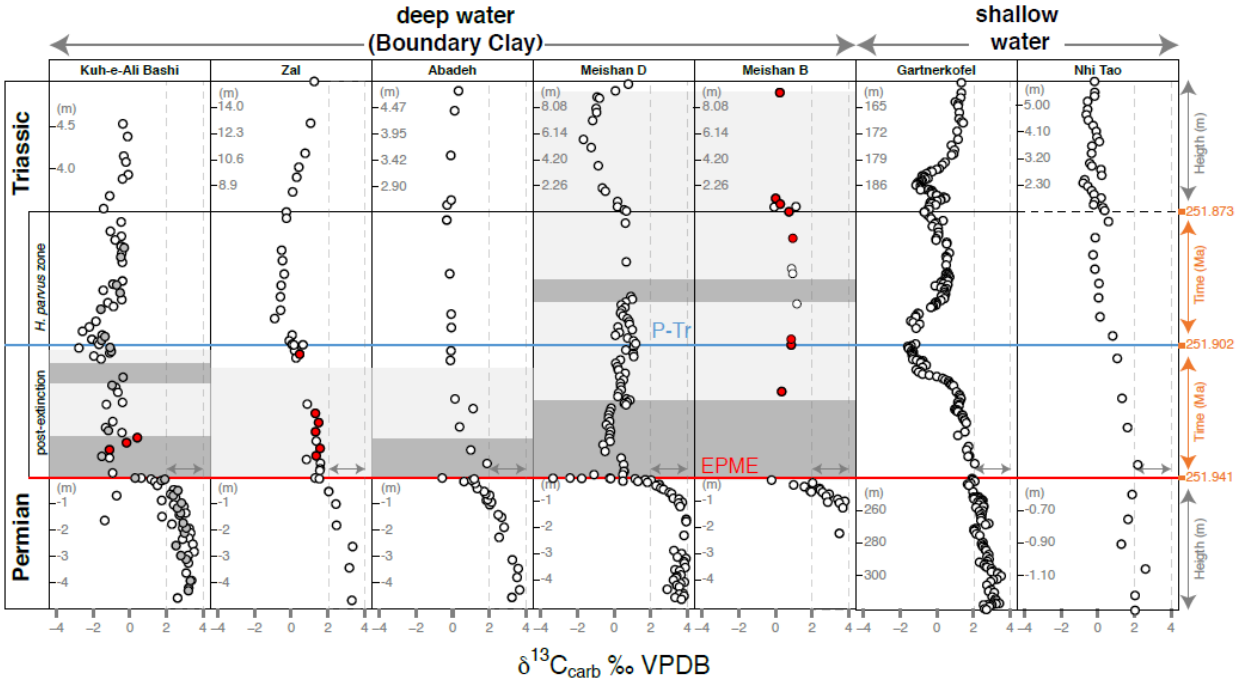

Figure 6

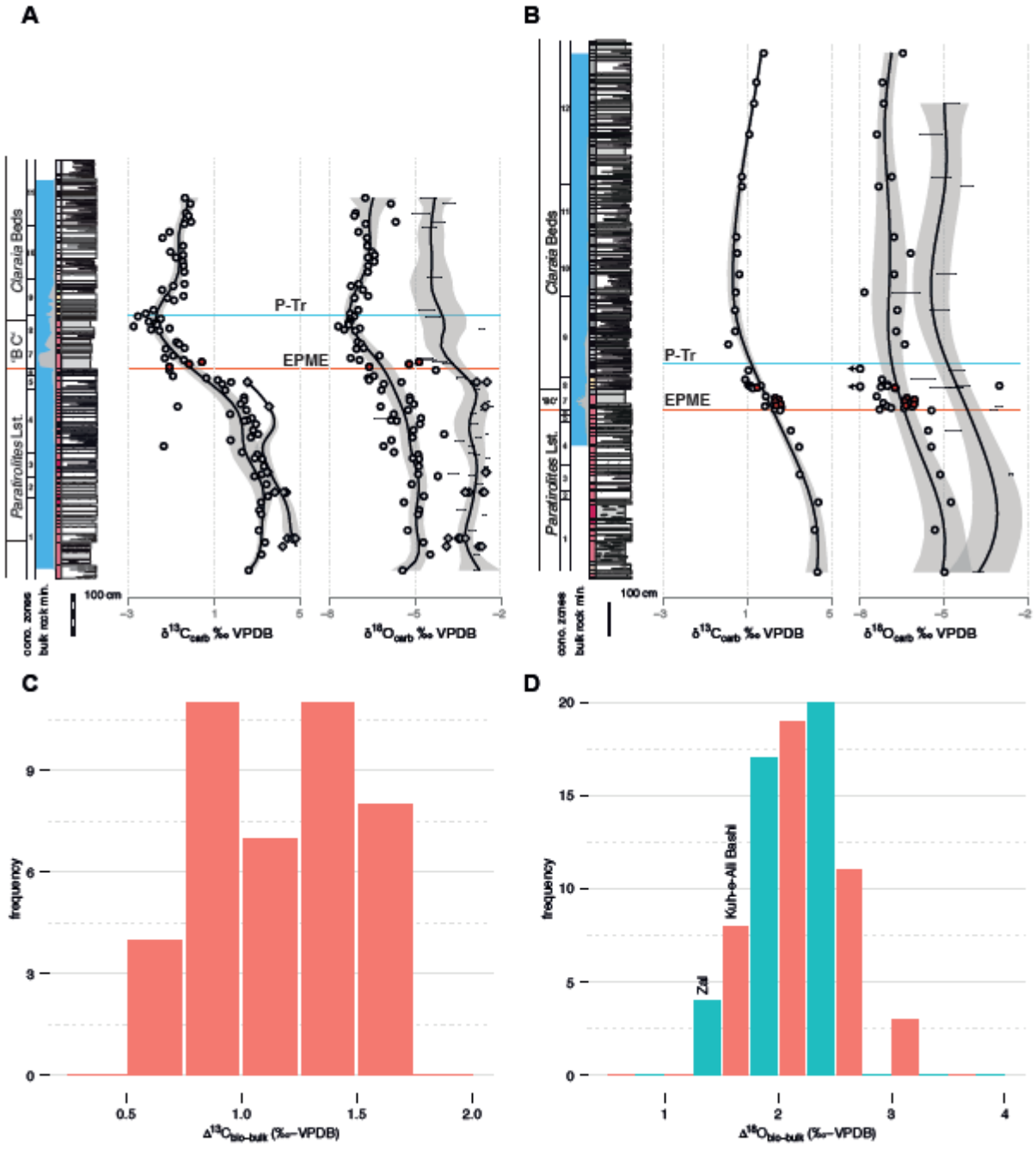

Figure 7

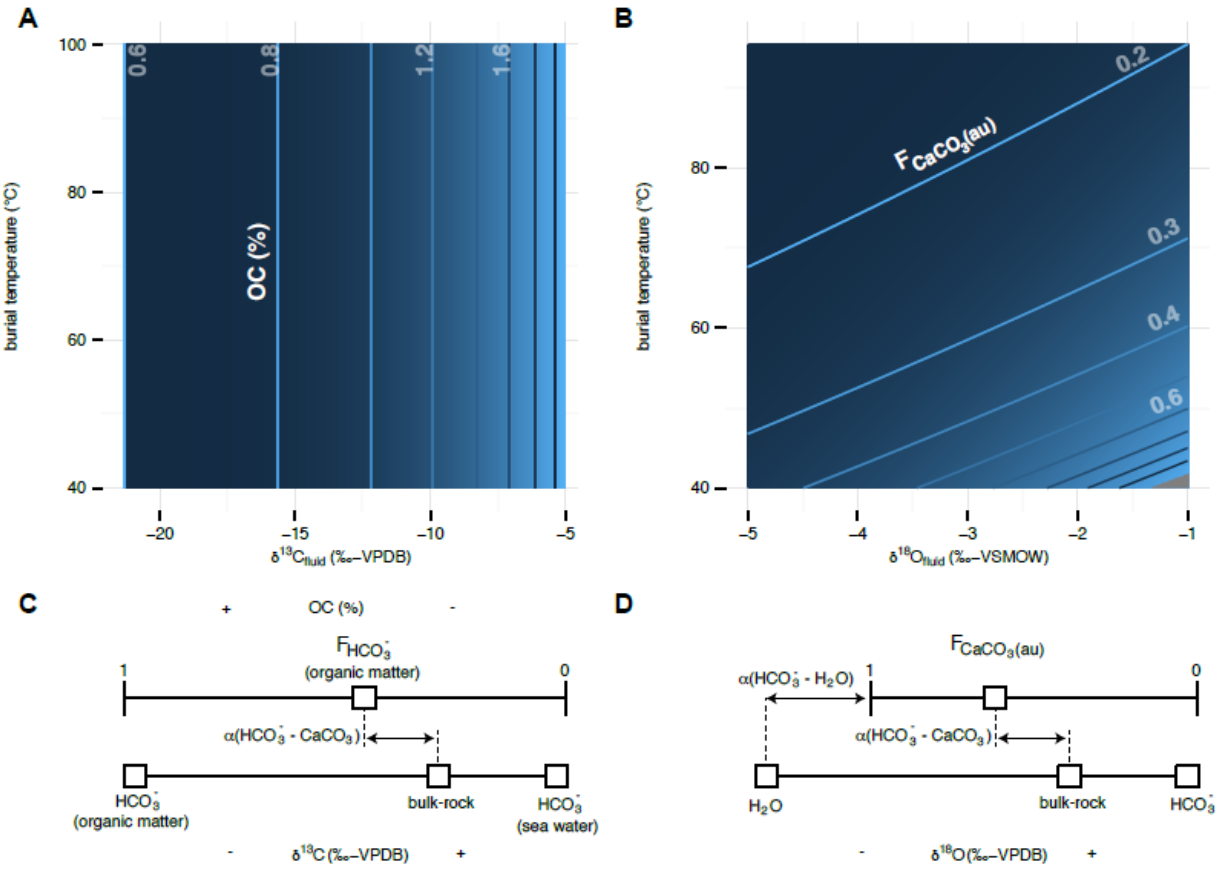

Figure 8

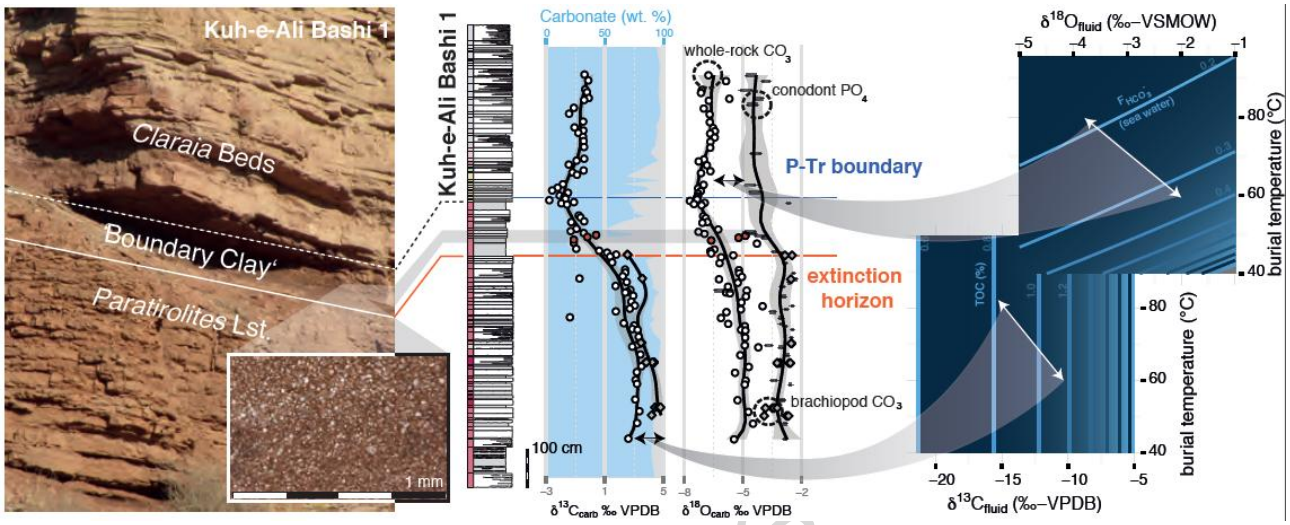

Graphical abstract

Highlights

- A high-resolution record of carbonate chemistry, including stable isotopes and elements
- Covariation in carbon-oxygen and trace elements are imperfect tracers of diagenesis
- A comparative bulk-rock—fossil approach can discern primary from diagenetic signals
- Elevated sea level preserves primary trends in bulk-rock carbon and oxygen isotopes
- Late-stage dolomitization alters primary carbonate chemistry at confined cm-scale intervals